Second, Third and Fourth Harmonic Generation at Crystalline Si(110) and Si(111) Surfaces

by

Roland Werner Kempf

Thesis

Presented to the Faculty of the Graduate School
of The University of Texas at Austin
in Partial Fulfillment
of the Requirements
for the Degree of

Master of Arts

The University of Texas at Austin
August 1998

Second, Third and Fourth Harmonic Generation at Crystalline Si(110) and Si(111) Surfaces

APPROVED BY
SUPERVISING COMMITTEE:

_____

_____

This work is dedicated to my parents for all their love and care.

Acknowledgments

At this point I want to thank Prof. Downer for the opportunity to work in his group, Mark Anderson and Yun-Shik Lee for the introduction to the laser system, my colleges Mikal Grimes, Philip Wilson, Erhard Gaul and Paul Le Blanc for their many tips and Prof. Aktsipetrov, Prof. Mishina, Dr. Lucymarie Mantese and Stephan Düsterer for the valuable discussions. Dr. Lucymarie Mantese gave me many suggestions and comments on this thesis.

I also want to express my thanks to those people, who made this year at the University of Texas possible at all, especially of course my parents, but also Prof. Scheer, Prof. Böhm, Prof. Yorke, Prof. Langhoff of the University of Würzburg and Prof. Fink of the University of Texas, who were responsible for this program. This work was supported by Texas ATP Grant No. 003658-178, the Robert Welch Foundation (Grant No. F-1038), AFOSR/DARPA MURI Contract No. F49620-95-1-0475, the NSF Science and Technology Center Program (CHE-8920210), and the AFOSR Contract No. F49620-95-C-0045.

The University of Texas at Austin Roland Kempf

August 1998

Table of Contents

List of Tables

List of Figures

Chapter 1

Introduction

Over the last 15 years, second harmonic generation (SHG) and related techniques such as sum- and difference frequency generation have been used as non-invasive probes of surfaces and interfaces. These second-order processes are dipole-forbidden in materials with an inversion center, however, this symmetry is broken at surfaces and interfaces making such second-order processes sensitive to these thin layers. In addition, with the development of solid state femtosecond lasers the conversion of second harmonic light on surfaces has improved dramatically. This can be shown by a simple scaling law that relates the polarization P with the peak electric field E and the pulse duration τ for the n-th harmonics:

$$P \propto \frac{E^n}{\tau^{n-1}} \tag{1.1}$$

Combining short pulses, a high repetition rate and moderate power it is now possible to generate fourth harmonic light from semiconductor surfaces below the damage threshold. To study the crystalline surface it is important to prevent optical damage, which requires that the average heating at the surface be minimized. Because the conversion rates of the fourth harmonic signal are significantly lower in comparison to second harmonic signals and because the signal scales with the fourth

power of the incident fields, high peak intensities and short pulses are necessary. The above requirements can be satisfied by using amplified femtosecond (fs) lasers. In the experiments discussed here, 200 fs pulses were used.

In this work, the complete analysis for 4-th harmonic generation of all crystal classes is presented. Also the azimuthal anisotropies of second, third and forth harmonic generation from Si(111) and Si(110) surfaces are shown which can be fitted well with the modeled dependence.

Chapter 2

Theory

2.1 Introduction to Linear Optics

The interaction of light with matter is mainly linear as long as the flux of photons is moderate ($1W/cm^2$). Under this condition the electrons are excited and upon relaxing primary as well as secondary photons are reflected.

Macroscopically this can be described using a harmonic oscillator model. It is assumed that only the electrons take part in the interaction and the remaining ions are omitted. Further the electrons are assumed to be placed in a dispersive harmonic oscillator potential that is driven by an electromagnetic wave. The equation of motion is then given by:

$$m\ddot{x} + 2\gamma\dot{x} + \omega_0^2 x = -\frac{e}{m}E(t) \tag{2.1}$$

where e and m are electron charge and mass, respectively. ω_0 is the resonance frequency of the transition and γ is a broadening parameter related to the excitation lifetime.

For a plain wave driving field, $E(t) = E_0 \exp[i(\omega t - kr)]$, the solution to Eq.(2.1) is:

$$x(\omega, r) = -\frac{e}{m}\frac{E_0}{\omega_0^2 - \omega^2 - 2i\omega\gamma}exp[i(\omega t - kr)] \tag{2.2}$$

The polarization is related to the linear susceptibility $\chi^{(1)}$ as:

$$P(\omega, r) = -Nex(\omega, r) = \chi^{(1)}(\omega)E(\omega) \tag{2.3}$$

and:

$$\chi^{(1)}(\omega) = N\frac{e^2}{m}\frac{1}{\omega_0^2 - \omega^2 - 2i\omega\gamma} \tag{2.4}$$

In three dimensions the potential may be directionally dependent and so the susceptibility that connects the electric field vector to the polarization vector is in general a tensor of rank two.

2.2 Nonlinear optical surface response

2.2.1 Quantum Mechanical Picture

When high electromagnetic field densities are applied to a medium, multi-photon excitations can take place. An electron may be excited to an intermediate level, which may be a virtual state, and then can be excited even further if the life time of this level is long in comparison to the time constant that governs the second absorption process. If this intermediate level is near a real state the conversion rate is enhanced due to a longer life time. This can take place several times until the electron relaxes again. During the relaxation process the excitation energy of the photon is emitted. Fig.(2.1)

As in linear radiation processes, some transitions are (dipole) forbidden. The non-linear selection rules depend strongly on the symmetry of the potential that the electrons experience. Symmetry properties will be discussed in more detail in section 2.3.

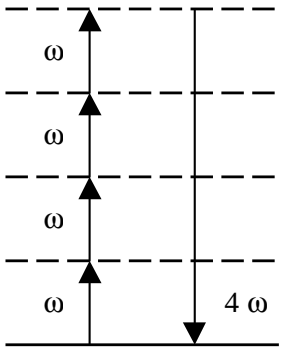

Figure 2.1: *Schematic Fourth Harmonic Generation (FHG) Process*

2.2.2 Anharmonic Oscillator Model

Bloembergen [1] used the anharmonic oscillator model to macroscopically describe harmonic generation. Deviations in the harmonic potential are taken into account and the potential is expanded as a power series. The equation of motion for the electrons is then given by:

$$m\ddot{x} + 2\gamma\dot{x} + \omega_0^2 x + \lambda x^2 + .. = -\frac{e}{m}E(t) \tag{2.5}$$

If the terms nonlinear in x are small they can be treated as a perturbation. The higher-order solutions have terms proportional to $e^{in\omega}E^n$ with integers n referring to the n-th harmonic, since the oscillating displacement results in a oscillating polarization that creates again an electromagnetic field with a frequency of $n\omega$. A more detailed description can be found in [3].

2.2.3 Nonlinear Dipole Susceptibility Tensor

The constant relating the n-th order polarization to the incoming electromagnetic fields is called the nonlinear susceptibility. It describes the generation of the non-

linear polarization by:

$$P = \chi_D^{(2)} : EE \tag{2.6}$$

As the anisotropy of the electronic potential varies along different directions the constants, relating the n components of the incoming electric field to the polarization vector, are in general a tensor of rank n+1.

2.2.4 Nonlinear Surface Dipole Susceptibility Tensor

At the surface of a crystal the electronic potential changes dramatically. Therefore, the interaction of the electrons with the electromagnetic field at the surfaces differs from the interaction in the bulk. To describe the additional resulting polarization a surface dipole susceptibility tensor $\chi^{(2),S}$ is introduced:

$$P = \chi_S^{(2)} : EE \tag{2.7}$$

Often the symmetry properties of the bulk are broken at the surface. Therefore, the shape of the tensor can be quite different compared to the bulk dipole susceptibility tensor.

2.2.5 DC induced higher harmonic signals

The bandstructure changes at the surface. The resulting electric DC field E_{DC} can couple with the incident electric fields and generate higher harmonics. The polarization contribution of this process can be described in two ways. For the first we use the third order nonlinear susceptibility tensor $\chi_B^{(3)}$:

$$P = \chi_B^{(3)} : EEE_{DC} \tag{2.8}$$

Since the DC field is in the z-direction in the surface coordinate system we can write it as $E_{DC} = f(z)\vec{e_z}$. If we insert this expression into Eq.(2.8) the 4^{th} rank tensor $\chi_B^{(3)}$ is reduced to an effective 3^{rd} rank tensor $\chi_{DC}^{(2)}(z)$. And we obtain:

$$P = \chi_{DC}^{(2)}(z) : EE \tag{2.9}$$

When we study the behaviour of this effective tensor under symmetry transformations we have to keep in mind that we already assigned a specific z-direction. Therefore we may only apply symmetry transformations that keep the z-direction unchanged. Since this effective tensor is like the surface dipole susceptibility tensor a tensor of rank 3 and in both cases only a limited number of symmetry transformations are allowed both tensors have the same symmetry properties.

2.2.6 Nonlinear Quadrupole Susceptibility Tensor

Gradients in the electric fields can also give rise to higher harmonic generation. In this case the nonlinear polarization is given by [4]:

$$P = \chi_Q^{(2)} : E\nabla E \tag{2.10}$$

In the plain wave approximation this equation can be written as:

$$P = i\chi_Q^{(2)} : EkE \tag{2.11}$$

Note that the rank of the tensor is n+2, as it connects the polarization vector to a gradient and n electric fields. Therefore, it can also resolve up to a (n+2)-fold rotational symmetry.

2.3 Symmetry Analysis of the Nonlinear Susceptibility Tensor

The nonlinear susceptibility tensors are described by a large number of elements. In principle there are $3^5 = 243$ complex elements in the case of the fourth-order nonlinear dipole susceptibility tensor. Fortunately the materials have some symmetry properties that can significantly reduce the number of independent tensor elements.

2.3.1 Intrinsic Symmetry of Harmonic Generation

Here, we consider harmonic signals where two, three or more photons of the *same* frequency couple within the material to emit a photon of double, threefold or higher frequency. The 2-nd order polarization is given by

$$P_i(2\omega) = \chi_{ijk}(2\omega, \omega, \omega)E_j(\omega)E_k(\omega) \tag{2.12}$$

If we interchange the last two dummy indices of χ_{ijk} we obtain an additional expression for the polarization:

$$P_i(2\omega) = \chi_{ikj}(2\omega, \omega, \omega)E_j(\omega)E_k(\omega) \tag{2.13}$$

Both equations must hold for arbitrary electric fields and each component of the polarization, so we can derive the intrinsic symmetry property:

$$\chi_{ijk} = \chi_{ikj} \tag{2.14}$$

In general, the last n indices of the (n+1)-th rank nonlinear susceptibility tensors can be permuted.

For the quadrupole tensor this intrinsic symmetry is not applicable, however, if the interacting waves come from one direction and have the same frequencies, i.e. have the same wave vectors, the gradients of all incoming electric fields are the same.

In this case the tensor of rank (n+2) is degenerated and the second index of the tensor can be used exclusively for the gradient and the last n indices referring to the electric fields can be permuted.

2.3.2 Spatial Symmetry

When the nonlinear medium has spatial symmetry, i.e. it is isotropic or has a certain point group, it is invariant under certain symmetry operations. This requires then that all the physical properties, i.e. the electronic potential and therefore the nonlinear susceptibility tensors of this material, have also to be invariant.

Taking Eq.(2.6) $P = \chi^{(2)} : EE$ and applying a symmetry operation S, we obtain, due to the invariance of χ:

$$SP = \chi : (SE)(SE) \tag{2.15}$$

$$\Rightarrow \quad P = \chi : EE \stackrel{!}{=} S^{-1}\chi : (SE)(SE) \tag{2.16}$$

Since the equation must hold for arbitrary electric fields, the condition for the susceptibility is:

$$\chi_{ijk} = S^{-1}_{il} S^{T}_{lm} S^{T}_{kn} \chi_{lmn} \tag{2.17}$$

A simple example is inversion symmetry where $S^{-1}_{ij} = S^{T}_{ij} = -\delta_{ij}$. Using Eq.(2.17), it follows: $\chi_{ijk} = -\chi_{ijk}$. Therefore χ_{ijk} vanishes completely in centro symmetric materials. In general, the generation of even harmonics are forbidden in these materials which enables us to study the quadrupole terms and the surface dipole susceptibility tensor.

Chapter 3

Program to calculate symmetry properties of χ

3.1 Calculation method

The most general susceptibility tensor of rank n can be described by 3^n independent numbers: its components. These components can be united to a 3^n-dimensional vector v_1. A vector notation is useful, since then all the tools of linear algebra are applicable. The components of the tensor have to satisfy homogeneous equations due to the invariance under certain symmetry operations (see Eq.(2.17)) and so do the components of the vector v_1. This equations can be written in matrix notation:

$$M_1 \cdot v_1 = 0 \tag{3.1}$$

We rewrite the vector v_1 as a linear combination of a basis X_1 with linear coefficients Λ:

$$v_1 = X_1 \cdot \Lambda \tag{3.2}$$

So we get:

$$M_1 \cdot v_1 = M_1 \cdot X_1 \cdot \Lambda = \tilde{M}_1 \cdot \Lambda = 0 \tag{3.3}$$

Now we want to find all possible linear combinations Λ that solve equation (3.3). The general solution Λ_1 is just the nullspace of $\tilde{M}_1 = M_1 \cdot X$. The new vector

v_2 that satisfies (3.3) is a linear combination of a new basis $X_2 = X_1 \cdot \Lambda_1$. If an additional symmetry operation applies, we replace v_1 now with $v_2 = X_2 \cdot \Lambda$ and look for a new nullspace Λ_2 of the new matrix $\tilde{M}_2 = M_2 \cdot v_2$, and so on. After the last symmetry operation is handled we write v as a linear combination of the last basis x and denote it again as a tensor χ.

If the intrinsic symmetry of harmonic generation is used we start already with a smaller basis that satisfies this condition.

Note: If the material is of a crystal class with many associated symmetry operations then it is only necessary to check, if the tensors are invariant under the operations that *generate* the symmetry group.

The algorithm in an overview:

- Set X_1 to a basis system, that actually can already be a subsystem of the vector space to satisfy the intrinsic symmetry.
- Generate the matrix $M_1 = [S_{il}^{-1} S_{lm}^T S_{kn}^T - \delta_{il}\delta_{jm}\delta_{kn}]$
- Find all Λ_1 that satisfy $M_1 X_1 \Lambda_1 = 0$ (Nullspace of $M_1 X_1$)
- Calculate $X_2 = X_1 \Lambda_1$
- Start with X_2 and the next symmetry matrix S at point 2

The program was written using Mathematica 3.0. When the first section of the program is evaluated the user is asked for the rank of the tensor and if the the intrinsic symmetry of the harmonic generation should be included. The crystal class of the material and/or additional symmetry operations can be specified as well. After the initial procedure, the program carries out the calculation sketched above.

The next section allows to print out all non-vanishing tensor elements and it gives their dependence, if they are separable. When the user chooses the orientation of the surface [1] the program computes the angular dependence of the generated harmonic field with respect to the non-vanishing tensor elements ('chi'), the linear ('lfx', 'lfy', 'lfz') and nonlinear ('fx', 'fy, 'fz') Fresnel factors and the surface orientation in reflection. When the user assigns values for those variables, the program can give a plot of the expected angular intensities.

Interesting variables that are accessible after the calculations are:

- chi: susceptibility tensor in tensor form
- x: last basis for v
- output1: all non-zero tensor elements
- output2: the separated tensor elements (if possible)
- ss, ps: angular dependence of the electric field in ss or ps polarization configuration
- spx, spz, ppx, ppz: angular dependence of the x or z component of the electric field in sp or pp polarization configuration

In principle, the program is capable of carrying out calculations for arbitrary large tensors and for any crystal class. The practical limit due to calculation time and memory usage are tensors up to a rank of five or, if the intrinsic symmetry is also used, up to a rank of six.

[1] The surface orientation must be given by the normal vector in the same coordinate system in which the tensor is described

The program for dipole tensors can be found in Appendix A. Appendix B describes how to modify the program to handle quadrupole tensors. The angular distribution for quadrupole components also depends on the values for the k vector component 'kx' along the surface and 'kz' perpendicular to the surface within the material. To get the plots those variables have to be set to a certain value as well. In this case the second index of χ always refers to the gradient.

3.2 Non zero Elements of $\chi^{(3,4)}$

This section[2] shows the non-zero elements for 3rd and 4th order nonlinear susceptibility tensors that also have the intrinsic symmetry of 3rd and 4th harmonic generation. The coordinate systems used are all Cartesian and were chosen as in the book of Wyckoff [2], except for the point group $3m$ to obtain the same results for 3rd harmonic generation as in the book 'Nonlinear Optics' by Shen [3]. If tensor elements differ only in the permutation of the last $(n-1)$ indices they are equal and so only one representative is listed. The point groups are denoted in international notation in the boxes and are followed by the number of non-zero elements and the number of independent parameters.

3.2.1 3rd harmonic dipole tensor elements

$\boxed{1, \overline{1}}$ 81 non-zero elements; 30 independent elements

all elements are independent (except intrinsic symmetry)

$\boxed{m, 2, 2/m}$ 41 non-zero elements; 16 independent elements

[2]Non-zero elements of $\chi^{(2)}$ are given in Refs. [3,5].

χ_{xxxx}, χ_{xxxz}, χ_{xxyy}, χ_{xxzz}, χ_{xyyz}, χ_{xzzz}, χ_{yxxy}, χ_{yxyz},

χ_{yyyy}, χ_{yyzz}, χ_{zxxx}, χ_{zxxz}, χ_{zxyy}, χ_{zxzz}, χ_{zyyz}, χ_{zzzz}

$\boxed{2mm,\ 222,\ mmm}$ 21 non-zero elements; 9 independent elements

χ_{xxxx}, χ_{xxyy}, χ_{xxzz}, χ_{yxxy}, χ_{yyyy}, χ_{yyzz}, χ_{zxxz}, χ_{zyyz}, χ_{zzzz}

$\boxed{\overline{4},\ 4,\ 4/m}$ 35 non-zero elements; 8 independent elements

$\chi_{xxxx} = \chi_{yyyy}$, $\chi_{xxxy} = -\chi_{yxyy}$, $\chi_{xxyy} = \chi_{yyxx}$, $\chi_{xxzz} = \chi_{yyzz}$,

$\chi_{xyyy} = -\chi_{yxxx}$, $\chi_{xyzz} = -\chi_{yxzz}$, $\chi_{zxxz} = \chi_{zyyz}$, χ_{zzzz}

$\boxed{\overline{4}2m,\ 4mm,\ 422,\ 4/mmm}$ 21 non-zero elements; 5 independent elements

$\chi_{xxxx} = \chi_{yyyy}$, χ_{xxyy}, $\chi_{xxzz} = \chi_{yyzz}$, $\chi_{zxxz} = \chi_{zyyz}$, χ_{zzzz}

$\boxed{23,\ m3}$ 21 non-zero elements; 3 independent elements

$\chi_{xxxx} = \chi_{yyyy} = \chi_{zzzz}$, $\chi_{xxyy} = \chi_{yyzz} = \chi_{zzxx}$, $\chi_{xxzz} = \chi_{yyxx} = \chi_{zzyy}$

$\boxed{\overline{4}3m,\ 432,\ m3m}$ 21 non-zero elements; 2 independent elements

$\chi_{xxxx} = \chi_{yyyy} = \chi_{zzzz}$, $\chi_{xxyy} = \chi_{yyzz} = \chi_{zzxx} = \chi_{xxzz} = \chi_{yyxx} = \chi_{zzyy}$

$\boxed{3,\ \overline{3}}$ 67 non-zero elements; 10 independent elements

$\chi_{xxxx} = 3\chi_{xxyy} = 3\chi_{yyxx} = \chi_{yyyy}$, $3\chi_{xxxy} = \chi_{xyyy} = -\chi_{yxxx} = -3\chi_{yxyy}$,

$\chi_{xxxz} = -\chi_{xyyz} = -\chi_{yxyz}$, $\chi_{xxyz} = \chi_{yxxz} = -\chi_{yyyz}$, $\chi_{xxzz} = \chi_{yyzz}$,

$\chi_{xyzz} = -\chi_{yxzz}$, $\chi_{zxxx} = -\chi_{zxyy}$, $\chi_{zxxy} = -\chi_{zyyy}$, $\chi_{zxxz} = \chi_{zyyz}$, χ_{zzzz}

$\boxed{3m,\ \overline{3}m}$ 37 non-zero elements; 6 independent elements

$\chi_{xxxx} = 3\chi_{xxyy} = 3\chi_{yyxx} = \chi_{yyyy}$, $\chi_{xxyz} = \chi_{yxxz} = -\chi_{yyyz}$,

$\chi_{xxzz} = \chi_{yyzz}$, $\chi_{zxxy} = -\chi_{zyyy}$, $\chi_{zxxz} = \chi_{zyyz}$, χ_{zzzz}

$\boxed{\overline{6},\ 6,\ 6/m}$ 35 non-zero elements; 6 independent elements

$\chi_{xxxx} = 3\chi_{xxyy} = 3\chi_{yxxy} = \chi_{yyyy}$, $3\chi_{xxxy} = \chi_{xyyy} = -\chi_{yxxx} = -3\chi_{yxyy}$,

$\chi_{xxzz} = \chi_{yyzz}$, $\chi_{xyzz} = -\chi_{yxzz}$, $\chi_{zxxz} = \chi_{zyyz}$, χ_{zzzz}

$\boxed{\overline{6}2m,\ 6mm,\ 622,\ 6/mmm}$ 21 non-zero elements; 4 independent elements

$\chi_{xxxx} = 3\chi_{xxyy} = \chi_{yyyy}$, $\chi_{xxzz} = \chi_{yyzz}$,$\chi_{zxxz} = \chi_{zyyz}$, χ_{zzzz}

$\boxed{isotropic}$ 21 non-zero elements; 1 independent element

$\chi_{xxxx} = 3\chi_{xxyy} = 3\chi_{xxzz} = 3\chi_{yxxy} = \chi_{yyyy} = 3\chi_{yyzz} = 3\chi_{zzxx} = 3\chi_{zzyy} = \chi_{zzzz}$

3.2.2 4th harmonic dipole tensor elements

$\boxed{1}$ 243 non-zero elements; 45

all elements are independent (except intrinsic symmetry)

$\boxed{\overline{1}, 2/m, mmm, 4/m, 4/mmm, m3, m3m, \overline{3}, \overline{3}m, 6/m, 6/mmm, isotropic}$

all elements vanish

$\boxed{m}$ 122 non-zero elements; 24 independent elements

χ_{xxxxx}, χ_{xxxxz}, χ_{xxxyy}, χ_{xxxzz}, χ_{xxyyz}, χ_{xxzzz}, χ_{xyyyy}, χ_{xyyzz},

χ_{xzzzz}, χ_{yxxxy}, χ_{yxxyz}, χ_{yxyyy}, χ_{yxyzz}, χ_{yyyyz}, χ_{yyzzz}, χ_{zxxxx},

χ_{zxxxz}, χ_{zxxyy}, χ_{zxxzz}, χ_{zxyyz}, χ_{zxzzz}, χ_{zyyyy}, χ_{zyyzz}, χ_{zzzzz}

$\boxed{2}$ 121 non-zero elements; 21 independent elements

χ_{xxxxy}, χ_{xxxyz}, χ_{xxyyy}, χ_{xxyzz}, χ_{xyyyz}, χ_{xyzzz}, χ_{yxxxx}, χ_{yxxxz}, χ_{yxxyy}, χ_{yxxzz}, χ_{yxyyz},

χ_{yxzzz}, χ_{yyyyy}, χ_{yyyzz}, χ_{yzzzz}, χ_{zxxxy}, χ_{zxxyz}, χ_{zxyyy}, χ_{zxyzz}, χ_{zyyyz}, χ_{zyzzz}

$\boxed{2mm}$ 61 non-zero elements; 12 independent elements

χ_{xxxxz}, χ_{xxyyz}, χ_{xxzzz}, χ_{yxxyz}, χ_{yyyyz}, χ_{yyzzz},

χ_{zxxxx}, χ_{zxxyy}, χ_{zxxzz}, χ_{zyyyy}, χ_{zyyzz}, χ_{zzzzz}

$\boxed{222}$ 60 non-zero elements; 9 independent elements

χ_{xxxyz}, χ_{xyyyz}, χ_{xyzzz}, χ_{yxxxz}, χ_{yxyyz}, χ_{yxzzz}, χ_{zxxxy}, χ_{zxyyy}, χ_{zxyzz}

$\boxed{\bar{4}}$ 114 non-zero elements; 10 independent elements

$\chi_{xxxxz} = -\chi_{yyyyz}$, $\chi_{xxxyz} = \chi_{yxyyz}$, $\chi_{xxyyz} = -\chi_{yxxyz}$, $\chi_{xxzzz} = -\chi_{yyzzz}$,

$\chi_{xyyyz} = \chi_{yxxxz}$, $\chi_{xyzzz} = \chi_{yxzzz}$, $\chi_{zxxxx} = -\chi_{zyyyy}$, $\chi_{zxxxy} = \chi_{zxyyy}$,

$\chi_{zxxzz} = -\chi_{zyyzz}$, χ_{zxyzz}

$\boxed{\bar{4}2m}$ 60 non-zero elements; 5 independent elements

$\chi_{xxxyz} = \chi_{yxyyz}$, $\chi_{xyyyz} = \chi_{yxxxz}$, $\chi_{xyzzz} = \chi_{yxzzz}$, $\chi_{zxxxy} = \chi_{zxyyy}$, χ_{zxyzz}

$\boxed{4}$ 109 non-zero elements; 11 independent elements

$\chi_{xxxxz} = \chi_{yyyyz}$, $\chi_{xxxyz} = -\chi_{yxyyz}$, $\chi_{xxyyz} = \chi_{yxxyz}$, $\chi_{xxzzz} = \chi_{yyzzz}$,

$\chi_{xyyyz} = -\chi_{yxxxz}$, $\chi_{xyzzz} = -\chi_{yxzzz}$, $\chi_{zxxxx} = \chi_{zyyyy}$, $\chi_{zxxxy} = -\chi_{zxyyy}$,

χ_{zxxyy}, $\chi_{zxxzz} = \chi_{zyyzz}$, χ_{zzzzz}

$\boxed{4mm}$ 61 non-zero elements; 7 independent elements

$\chi_{xxxxz} = \chi_{yyyyz}$, $\chi_{xxyyz} = \chi_{yxxyz}$, $\chi_{xxzzz} = \chi_{yyzzz}$, $\chi_{zxxxx} = \chi_{zyyyy}$,

χ_{zxxyy}, $\chi_{zxxzz} = \chi_{zyyzz}$, χ_{zzzzz}

$\boxed{422}$ 48 non-zero elements; 4 independent elements

$\chi_{xxxyz} = -\chi_{yxyyz}$, $\chi_{xyyyz} = -\chi_{yxxxz}$, $\chi_{xyzzz} = -\chi_{yxzzz}$, $\chi_{zxxxy} = -\chi_{zxyyy}$

$\boxed{23}$ 60 non-zero elements; 3 independent elements

$\chi_{xxxyz} = \chi_{yxyyz} = \chi_{zxyzz}$, $\chi_{xyyyz} = \chi_{yxzzz} = \chi_{zxxxy}$, $\chi_{xyzzz} = \chi_{yxzzz} = \chi_{zxyyy}$

$\boxed{\bar{4}3m}$ 60 non-zero elements; 2 independent elements

$\chi_{xxxyz} = \chi_{yxyyz} = \chi_{zxyzz}$, $\chi_{xyyyz} = \chi_{yxzzz} = \chi_{zxxxy} = \chi_{xyzzz} = \chi_{yxzzz} = \chi_{zxyyy}$

$\boxed{432}$ 24 non-zero elements; 1 independent element

$\chi_{xyyyz} = -\chi_{xyzzz} = -\chi_{yxxxz} = \chi_{yxzzz} = \chi_{zxxxy} = -\chi_{zxyyy}$

$\boxed{3}$ 213 non-zero elements; 15 independent elements

$\chi_{xxxxz} = 3\chi_{xxyyz} = 3\chi_{yxxyz} = \chi_{yyyyz}$, $3\chi_{xxxyz} = \chi_{xyyyz} = -\chi_{yxxxz} - \chi_{yxyyz}$,

$\chi_{xxxzz} = -\chi_{xyyzz} = -\chi_{yxyzz}$, $\chi_{xxyzz} = \chi_{yxxzz} = -\chi_{yyyzz}$, $\chi_{xxzzz} = \chi_{yyzzz}$,

$\chi_{xyzzz} = -\chi_{yxzzz}$, $\chi_{zxxxx} = 3\chi_{zxxyy} = \chi_{zyyyy}$, $\chi_{zxxxz} = -\chi_{zxyyz}$,

$\chi_{zxxyz} = -\chi_{zyyyz}$,$\chi_{zxxzz} = \chi_{zyyzz}$, χ_{zzzzz}

χ_{xxxxx}, χ_{yxyyy}, χ_{xxxxy}, χ_{yxxyy}

The following non-zero tensor elements can be expressed as linear combinations of the above independent elements

$\chi_{xxxyy} = \chi_{xxxxx} + 2\chi_{yxyyy}$, $\chi_{xyyyy} = 3\chi_{xxxx} - 4\chi_{yxyyy}$,

$\chi_{yxxxy} = -2\chi_{xxxxx} - 3\chi_{yxyyy}$, $\chi_{xxyyy} = \chi_{xxxxy} + 2\chi_{yxxyy}$,

$\chi_{yyyyy} = -2\chi_{xxxxy} + \chi_{yxxyy}$, $\chi_{yxxxx} = 2\chi_{xxxxy} + 3\chi_{yxxyy}$

$\boxed{3m}$ 117 non-zero elements; 9 independent elements

$\chi_{xxxxz} = 3\chi_{xxyyz} = 3\chi_{yxxyz} = \chi_{yyyyz}$, $\chi_{xxyzz} = \chi_{yxxzz} = -\chi_{yyyzz}$,

$\chi_{xxzzz} = \chi_{yyzzz}$, $\chi_{zxxxx} = 3\chi_{zxxyy} = \chi_{zyyyy}$, $\chi_{zxxyz} = -\chi_{zyyyz}$,

$\chi_{zxxzz} = \chi_{zyyzz}$, χ_{zzzzz}, χ_{xxxxy}, χ_{yxxyy}

The following non-zero tensor elements can be expressed as linear combinations of the above independent elements

$\chi_{xxyyy} = \chi_{xxxxy} + 2\chi_{yxxyy}$, $\chi_{yyyyy} = -2\chi_{xxxxy} + \chi_{yxxyy}$, $\chi_{yxxxx} = 2\chi_{xxxxy} + 3\chi_{yxxyy}$

$\boxed{\bar{6}}$ 112 non-zero elements; 8 independent elements

$\chi_{xxxzz} = -\chi_{xyyzz} = -\chi_{yxyzz}$, $\chi_{xxyzz} = \chi_{yxxzz} = -\chi_{yyyzz}$, $\chi_{zxxxz} = -\chi_{zxyyz}$,

$\chi_{zxxyz} = \chi_{zyyyz}$, χ_{xxxxx}, χ_{yxyyy}, χ_{xxxxy}, χ_{yxxyy}

The following non-zero tensor elements can be expressed as linear combinations of the above independent elements

$\chi_{xxxyy} = \chi_{xxxxx} + 2\chi_{yxyyy}$, $\chi_{xyyyy} = 3\chi_{xxxxx} - 4\chi_{yxyyy}$,

$\chi_{yxxxy} = -2\chi_{xxxxx} - 3\chi_{yxyyy}$, $\chi_{xxyyy} = \chi_{xxxxy} + 2\chi_{yxxyy}$,

$\chi_{yyyyy} = -2\chi_{xxxxy} + \chi_{yxxyy}$, $\chi_{yxxxx} = 2\chi_{xxxxy} + 3\chi_{yxxyy}$

$\boxed{\bar{6}m2}$ 56 non-zero elements; 4 independent elements

χ_{xxxxx}, χ_{yxyyy}, $\chi_{xxxzz} = -\chi_{xyyzz} = -\chi_{yxyzz}$, $\chi_{zxxxz} = -\chi_{zxyyz}$

The following non-zero tensor elements can be expressed as linear combinations of the above independent elements

$\chi_{xxxyy} = \chi_{xxxxx} + 2\chi_{yxyyy}$, $\chi_{xyyyy} = 3\chi_{xxxxx} - 4\chi_{yxyyy}$, $\chi_{yxxxy} = -2\chi_{xxxxx} - 3\chi_{yxyyy}$

$\boxed{6}$ 101 non-zero elements; 7 independent elements

$\chi_{xxxxz} = 3\chi_{xxyyz} = 3\chi_{yxxyz} = \chi_{yyyyz}$, $\chi_{xyyyz} = 3\chi_{xxxyz} = -3\chi_{yxyyz} = -\chi_{yxxxz}$,

$\chi_{xxzzz} = \chi_{yyzzz}$, $\chi_{xyzzz} = -\chi_{yxzzz}$, $\chi_{zxxxx} = 3\chi_{zxxyy} = \chi_{zyyyy}$,

$\chi_{zxxzz} = \chi_{zyyzz}$, χ_{zzzzz}

$\boxed{6mm}$ 61 non-zero elements; 5 independent elements

$\chi_{xxxxz} = 3\chi_{xxyyz} = 3\chi_{yxxyz}$, $\chi_{xxzzz} = \chi_{yyzzz}$,

$\chi_{zxxxx} = 3\chi_{zxxyy} = \chi_{zyyyy}$, $\chi_{zxxzz} = \chi_{zyyzz}$, χ_{zzzzz}

$\boxed{622}$ 40 non-zero elements; 2 independent elements

$\chi_{xyyyz} = 3\chi_{xxxyz} = -3\chi_{yxyyz} = -\chi_{yxxxz}$, $\chi_{xyzzz} = -\chi_{yxzzz}$

3.2.3 Quadrupole tensor elements

Since silicon is a centro-symmetric material its SHG and FHG dipole tensors are zero and therefore the highest order bulk terms are determined by the quadrupole tensor. This contribution to the higher harmonics competes with the surface dipole terms. For THG the bulk dipole term is dominant and the surface dipole and bulk quadrupole contributions can be neglected. Appendix E lists the non-zero tensor elements of the 6^{th} rank tensor $\chi^{(4)Q}_{ijklmn}$ describing the bulk quadrupole contribution to FHG for a crystal with $m3m$ symmetry. Bulk quadrupole tensors for SHG are given in Ref [5].

3.3 Angular dependence of the signal

The following sections tabulate the lowest order contributing terms to the SHG (surface dipole, bulk quadrupole), THG (bulk dipole) and FHG (surface dipole, bulk quadrupole) for Si(110) and Si(111). They are used to model the experimental results in sections and 4.5 and 4.6.

To describe the signals four different coordinate systems were used. The crystallographic coordinate system (x, y, z) has the axis [100], [010] and [001]. The surface coordinate system axis in the case of Si(110) correspond to the crystallographic directions $[1\bar{1}0]$, $[00\bar{1}]$ and [110], respectively. For Si(111) the surface coordinates (x'', y'', z'') correspond to the crystallographic directions $[2\bar{1}\bar{1}]$, $[01\bar{1}]$ and [111]. The laboratory coordinate system (x_0, y_0, z_0) is related to the surface coordinate system by a rotational transformation. The susceptibility tensors transform as:

$$\hat{\chi}^S = \tilde{R}^{-1}\hat{\chi}^L\tilde{R} \tag{3.4}$$

with

$$\tilde{R} = \begin{pmatrix} \cos(\phi) & -\sin(\phi) & 0 \\ \sin(\phi) & \cos(\phi) & 0 \\ 0 & 0 & 1 \end{pmatrix} \tag{3.5}$$

The surface normal (crystallographic [110] or [111]) coincidence with z_0. The angle ϕ is the rotation angle between the surface coordinate system and the rotated laboratory system.

The abbreviations used in the tables are defined in terms of the angle of incident θ and the susceptibility (ϵ, ϵ_n) of the fundamental and n^{th} harmonic, respectively, and are defined in the laboratory frame (x_0, y_0, z_0) as follows: The linear

Fresnel factors ($f_{x,y,z}$) that relate the components of the electric field inside the medium to the amplitude of the electric field outside the medium are given by:

$$f_y = \frac{2\cos\theta}{\cos\theta + \sqrt{\epsilon - \sin^2\theta}} \tag{3.6}$$

$$f_x = \frac{2\cos\theta\sqrt{\epsilon - \sin^2\theta}}{\epsilon\cos\theta + \sqrt{\epsilon - \sin^2\theta}} \tag{3.7}$$

$$f_z = \frac{2\sin\theta}{\epsilon\cos\theta + \sqrt{\epsilon - \sin^2\theta}} \tag{3.8}$$

The nonlinear Fresnel factors ($f^{(n)}_{x,y,z}$) for the n^{th} harmonic signal that relate the nonlinear polarization P^{NL} inside the medium to the nonlinear wave E_n outside the medium can be found in Ref. [7]. For S and P-polarized higher harmonics we obtain:

$$\vec{E}^S_n = f^{(n)}_y P_S \vec{e}_y \tag{3.9}$$

$$\vec{E}^S_n = f^{(n)}_x P_x \vec{e}_x + f^{(n)}_z P_z \vec{e}_z \tag{3.10}$$

with

$$f^{(n)}_y = \frac{4\pi}{\epsilon - \epsilon_n}\frac{\sqrt{\epsilon_n - \sin^2\theta} - \sqrt{\epsilon - \sin^2\theta}}{\sqrt{\epsilon_n - \sin^2\theta} + \cos\theta} \tag{3.11}$$

$$f^{(n)}_x = \frac{4\pi\sqrt{\epsilon_n - \sin^2\theta}}{(\sqrt{\epsilon_n - \sin^2\theta} + \sqrt{\epsilon - \sin^2\theta})(\sqrt{\epsilon_n - \sin^2\theta} + \cos\theta)} \tag{3.12}$$

$$f^{(n)}_z = \frac{4\pi\sin\theta}{(\sqrt{\epsilon_n - \sin^2\theta} + \sqrt{\epsilon - \sin^2\theta})(\sqrt{\epsilon_n - \sin^2\theta} + \cos\theta)} \tag{3.13}$$

The components of the wave vector inside the medium (k_x, k_z) that are interesting in quadrupole contributions are given by:

$$k_x = \frac{\omega}{c}\sin\theta \tag{3.14}$$

$$k_z = \frac{\omega}{c}\sqrt{\epsilon_n - \sin^2\theta} \tag{3.15}$$

The amplitude of the electric field of the incident wave was set to unity.

3.3.1 Angular dependence of the signal from Si(110)

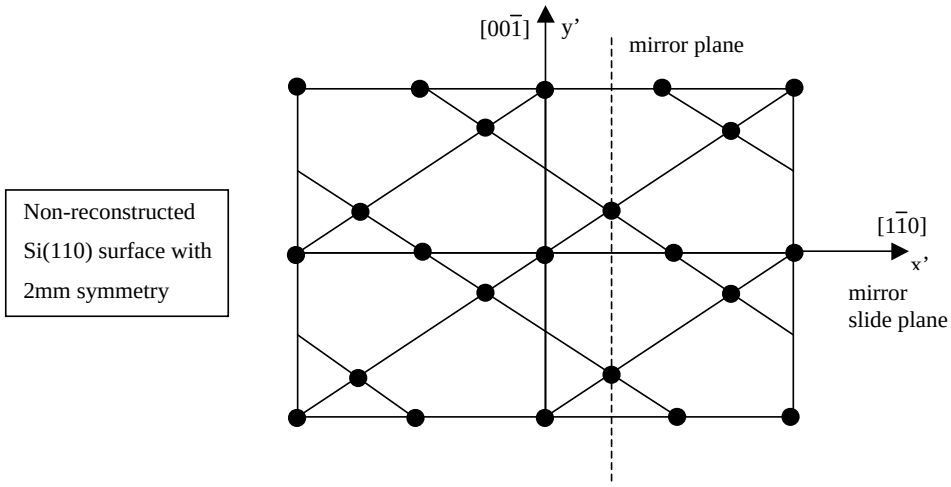

Figure 3.1: *Definition of surface coordinate system Si(110)*

Table 3.1: *SHG surface dipole (D^S) and bulk quadrupole (Q^B) contributions of Si(110)*

		Isotropic	Anisotropic (2ϕ)	Anisotropic (4ϕ)
S-in, S-out	D^S	0	0	0
S-in, S-out	Q^B	0	$b^Q_{SS}\sin 2\phi$	$c^Q_{PP}\sin 4\phi$
S-in, P-out	D^S	a^S_{SP}	$b^S_{SP}\cos 2\phi$	0
S-in, P-out	Q^B	a^Q_{SP}	$b^Q_{SP}\cos 2\phi$	$c^Q_{SP}\cos 4\phi$
P-in, S-out	D^S	0	$b^S_{PS}\sin 2\phi$	0
P-in, S-out	Q^B	0	$b^Q_{PS}\sin 2\phi$	$c^Q_{PS}\sin 4\phi$
P-in, P-out	D^S	a^S_{PP}	$b^S_{PP}\cos 2\phi$	0
P-in, P-out	Q^B	a^Q_{PP}	$b^Q_{PP}\cos 2\phi$	$c^Q_{PP}\cos 4\phi$

$$
\begin{aligned}
a^S_{SP} &= \frac{1}{2} f^{(2)}_z (\chi^S_{z'x'x'} + \chi^S_{z'y'y'}) f_y^2 \\
b^S_{SP} &= -\frac{1}{2} f^{(2)}_z (\chi^S_{z'x'x'} - \chi^S_{z'y'y'}) f_y^2 \\
b^S_{PS} &= -f^{(2)}_y (\chi^S_{x'x'z'} - \chi^S_{y'y'z'}) f_x f_z \\
a^S_{PP} &= f^{(2)}_x (\chi^S_{x'x'z'} + \chi^S_{y'y'z'}) f_x f_z + \frac{1}{2} f^{(2)}_z (\chi^S_{z'x'x'} f_x^2 + \chi^S_{z'y'y'} f_x^2 + 2\chi^S_{z'z'z'} f_z^2) \\
b^S_{PP} &= -f^{(2)}_x (\chi^S_{x'x'z'} - \chi^S_{y'y'z'}) f_x f_z + \frac{1}{2} f^{(2)}_z (\chi^S_{z'x'x'} - \chi^S_{z'y'y'}) f_x^2
\end{aligned}
$$

With 5 independent tensor elements (corresponding to 2mm symmetry):

$\chi^S_{x'x'z'}$, $\chi^S_{y'y'z'}$, $\chi^S_{z'x'x'}$, $\chi^S_{z'y'y'}$, $\chi^S_{z'z'z'}$

$$
\begin{aligned}
b^Q_{SS} &= \frac{1}{8} f_y^{(2)} (\chi^Q_{xxxx} - \chi^Q_{xxyy} - 2\chi^Q_{xyxy}) k_x f_y^2 \\
c^Q_{SS} &= \frac{3}{16} f_y^{(2)} (\chi^Q_{xxxx} - \chi^Q_{xxyy} - 2\chi^Q_{xyxy}) k_x f_y^2 \\
a^Q_{SP} &= \frac{1}{16} f_x^{(2)} (3\chi^Q_{xxxx} + 13\chi^Q_{xxyy} - 6\chi^Q_{xyxy}) k_x f_y^2 + \\
&\quad + \frac{1}{4} f_z^{(2)} (2\chi^Q_{xxxx} + 3\chi^Q_{xxyy} - 2\chi^Q_{xyxy}) k_z f_y^2 \\
b^Q_{SP} &= -\frac{1}{4} f_z^{(2)} (\chi^Q_{xxxx} - \chi^Q_{xxyy} - 2\chi^Q_{xyxy}) k_z f_y^2 \\
c^Q_{SP} &= -\frac{3}{16} f_x^{(2)} (\chi^Q_{xxxx} - \chi^Q_{xxyy} - 2\chi^Q_{xyxy}) k_x f_y^2 \\
b^Q_{PS} &= -\frac{1}{8} f_y^{(2)} (\chi^Q_{xxxx} - \chi^Q_{xxyy} - 2\chi^Q_{xyxy}) (k_x f_x^2 - 4k_z f_x f_z - 2k_z f_z^2) \\
c^Q_{PS} &= -\frac{3}{16} f_y^{(2)} (\chi^Q_{xxxx} - \chi^Q_{xxyy} - 2\chi^Q_{xyxy}) k_x f_x^2 \\
a^Q_{PP} &= \frac{1}{16} f_x^{(2)} (9\chi^Q_{xxxx} + 7\chi^Q_{xxyy} + 14\chi^Q_{xyxy}) k_x f_x^2 + \\
&\quad + \frac{1}{2} (f_x^{(2)} + f_z^{(2)}) (\chi^Q_{xxxx} - \chi^Q_{xxyy} + 2\chi^Q_{xyxy}) k_x f_x f_z + \\
&\quad + \frac{1}{4} f_x^{(2)} (\chi^Q_{xxxx} + 2\chi^Q_{xxyy} + 2\chi^Q_{xyxy}) k_x f_x f_z + \\
&\quad + \frac{1}{4} f_z^{(2)} (\chi^Q_{xxxx} + 3\chi^Q_{xxyy} - 2\chi^Q_{xyxy}) k_z f_x^2 + \\
&\quad + \frac{1}{2} f_z^{(2)} (\chi^Q_{xxxx} + 2\chi^Q_{xxyy} + 4\chi^Q_{xyxy}) k_z f_z^2 \\
b^Q_{PP} &= -\frac{1}{4} f_x^{(2)} (\chi^Q_{xxxx} - \chi^Q_{xxyy} - 2\chi^Q_{xyxy}) k_x f_x^2 + \\
&\quad + \frac{1}{4} f_x^{(2)} (\chi^Q_{xxxx} - \chi^Q_{xxyy} + 2\chi^Q_{xyxy}) (-2k_z f_x f_z + k_x f_z^2) + \\
&\quad + \frac{1}{4} f_z^{(2)} (\chi^Q_{xxxx} - \chi^Q_{xxyy} - 2\chi^Q_{xyxy}) (k_z f_x + 2k_x f_z) f_x \\
c^Q_{PP} &= \frac{\sqrt{2}}{6} f_x^{(2)} (\chi^Q_{xxxx} - \chi^Q_{xxyy} - 2\chi^Q_{xyxy}) (k_z f_x + 2k_x f_z) f_x + \\
&\quad + \frac{\sqrt{2}}{6} f_z^{(2)} (\chi^Q_{xxxx} - \chi^Q_{xxyy} - 2\chi^Q_{xyxy}) k_x f_x^2
\end{aligned}
$$

With 3 independent tensor elements (corresponding to m3m symmetry):

$\chi^Q_{xxxx} = \chi^Q_{yyyy} = \chi^Q_{zzzz}$, $\chi^Q_{xxyy} = \chi^Q_{xxzz} = \chi^Q_{yyxx} = \chi^Q_{yyzz} = \chi^Q_{zzxx} = \chi^Q_{zzyy}$, $\chi^Q_{xyxy} = \chi^Q_{xzxz} = \chi^Q_{yxxy} = \chi^Q_{yzyz} = \chi^Q_{zxxz} = \chi^Q_{zyyz}$

Table 3.2: *THG bulk dipole contributions of Si(110)*

	Isotropic	Anisotropic (2ϕ)	Anisotropic (4ϕ)
S-in, S-out	a_{SS}	$b_{SS}\cos 2\phi$	$c_{SS}\cos 4\phi$
S-in, P-out	0	$b_{SP}\sin 2\phi$	$c_{SP}\sin 4\phi$
P-in, S-out	0	$b_{PS}\sin 2\phi$	$c_{PS}\sin 4\phi$
P-in, P-out	a_{PP}	$b_{PP}\cos 2\phi$	$c_{PP}\cos 4\phi$

$$
\begin{aligned}
a_{SS} &= \frac{3}{16} f_y^{(3)} (3\chi_{xxxx} + 7\chi_{xxyy}) f_y^3 \\
b_{SS} &= -\frac{1}{4} f_y^{(3)} (\chi_{xxxx} - 3\chi_{xxyy}) f_y^3 \\
c_{SS} &= \frac{3}{16} f_y^{(3)} (\chi_{xxxx} - 3\chi_{xxyy}) f_y^3 \\
b_{SP} &= -\frac{1}{8} f_x^{(3)} (\chi_{xxxx} - 3\chi_{xxyy}) f_y^3 \\
c_{SP} &= \frac{3}{16} f_x^{(3)} (\chi_{xxxx} - 3\chi_{xxyy}) f_y^3 \\
b_{PS} &= -\frac{1}{8} f_y^{(3)} (\chi_{xxxx} - 3\chi_{xxyy}) (f_x^2 - 6 f_z^2) f_x \\
c_{PS} &= -\frac{3}{16} f_y^{(3)} (\chi_{xxxx} - 3\chi_{xxyy}) f_x^3 \\
a_{PP} &= \frac{3}{16} f_x^{(3)} ((3\chi_{xxxx} + 7\chi_{xxyy}) f_x^2 + 4(\chi_{xxxx} + \chi_{xxyy}) f_z^2) f_x + \\
&\quad + \frac{1}{4} f_z^{(3)} (3(\chi_{xxxx} + \chi_{xxyy}) f_x^2 + 2(\chi_{xxxx} + 3\chi_{xxyy}) f_z^2) f_z \\
b_{PP} &= \frac{1}{4} (\chi_{xxxx} - 3\chi_{xxyy}) (f_x^{(3)} (f_x^2 - 3 f_z^2) f_x - 3 f_z^{(3)} f_x^2 f_z) \\
c_{PP} &= \frac{3}{16} f_x^{(3)} (\chi_{xxxx} - 3\chi_{xxyy}) f_x^3
\end{aligned}
$$

With 2 independent tensor elements (corresponding to m3m symmetry):

$\chi_{xxxx} = \chi_{yyyy} = \chi_{zzzz}$

$\chi_{xxyy} = \chi_{xxzz} = \chi_{yyxx} = \chi_{yyzz} = \chi_{zzxx} = \chi_{zzyy}$

Table 3.3: *FHG surface dipole (D^S) and bulk quadrupole (Q^B) contributions of Si(110)*

		Isotropic	Anisotr. (2ϕ)	Anisotr. (4ϕ)	Anisotr. (6ϕ)
S-in,S-out	D^S	0	0	0	0
S-in,S-out	Q^B	0	$b^Q_{SS}\sin 2\phi$	$c^Q_{PP}\sin 4\phi$	$d^Q_{PP}\sin 6\phi$
S-in,P-out	D^S	a^S_{SP}	$b^S_{SP}\cos 2\phi$	$c^S_{SP}\cos 4\phi$	0
S-in,P-out	Q^B	a^Q_{SP}	$b^Q_{SP}\cos 2\phi$	$c^Q_{SP}\cos 4\phi$	$d^Q_{SP}\cos 6\phi$
P-in,S-out	D^S	0	$b^S_{PS}\sin 2\phi$	$c^S_{PS}\sin 4\phi$	0
P-in,S-out	Q^B	0	$b^Q_{PS}\sin 2\phi$	$c^Q_{PS}\sin 4\phi$	$d^Q_{PS}\sin 6\phi$
P-in,P-out	D^S	a^S_{PP}	$b^S_{PP}\cos 2\phi$	$c^S_{PP}\cos 4\phi$	0
P-in,P-out	Q^B	a^Q_{PP}	$b^Q_{PP}\cos 2\phi$	$c^Q_{PP}\cos 4\phi$	$d^Q_{PP}\cos 6\phi$

$$
\begin{aligned}
a^S_{SP} &= \frac{3}{8} f^{(4)}_z (\chi^S_{z'x'x'x'} + 2\chi^S_{z'x'x'y'y'} + \chi^S_{z'y'y'y'y'}) f^4_y \\
b^S_{SP} &= \frac{1}{2} f^{(4)}_z (\chi^S_{z'y'y'y'y'} - \chi^S_{z'x'x'x'x'}) f^4_y \\
c^S_{SP} &= \frac{1}{8} f^{(4)}_z (\chi^S_{z'x'x'x'x'} - 6\chi^S_{z'x'x'y'y'} + \chi^S_{z'y'y'y'y'}) f^4_y \\
b^S_{PS} &= -f^{(4)}_y (\chi^S_{x'x'x'x'z'} + 3\chi^S_{x'x'y'y'z'} - 3\chi^S_{y'x'x'y'z'} - \chi^S_{y'y'y'y'z'}) f^3_x f_z - \\
&\quad -2 f^{(4)}_y (\chi^S_{x'x'z'z'z'} - \chi^S_{y'y'z'z'z'}) f_x f^3_z \\
c^S_{PS} &= -\frac{1}{2} f^{(4)}_y (\chi^S_{x'x'x'x'z'} - 3\chi^S_{x'x'y'y'z'} - 3\chi^S_{y'x'x'y'z'} + \chi^S_{y'y'y'y'z'}) f^3_x f_z \\
a^S_{PP} &= \frac{3}{2} f^{(4)}_x (\chi^S_{x'x'x'x'z'} + \chi^S_{x'x'y'y'z'} + \chi^S_{y'x'x'y'z'} + \chi^S_{y'y'y'y'z'}) f^3_x f_z + \\
&\quad +2 f^{(4)}_x (\chi^S_{x'x'z'z'z'} + \chi^S_{y'y'z'z'z'}) f_x f^3_z + \\
&\quad +\frac{3}{8} f^{(4)}_z (\chi^S_{z'x'x'x'x'} + 2\chi^S_{z'x'x'y'y'} + \chi^S_{z'y'y'y'y'}) f^4_x + \\
&\quad +f^{(4)}_z (3(\chi^S_{z'x'x'z'z'} + \chi^S_{z'y'y'z'z'}) f^2_x f^2_z + \chi^S_{z'y'y'y'y'} f^4_z)
\end{aligned}
$$

$$
\begin{aligned}
b^S_{PP} &= 2f_x^{(4)}((\chi^S_{x'x'x'x'z'} - \chi^S_{y'y'y'y'z'})f_x^2 + (\chi^S_{x'x'z'z'z'} - \chi^S_{y'y'z'z'z'})f_z^2)f_x f_z + \\
&\quad + \frac{1}{2}f_z^{(4)}((\chi^S_{z'x'x'x'x'} - \chi^S_{z'y'y'y'y'})f_x^4 + (\chi^S_{z'x'x'z'z'} - \chi^S_{z'y'y'z'z'})f_x^2 f_z^2) \\
c^S_{PP} &= \frac{1}{2}f_x^{(4)}(\chi^S_{x'x'x'x'z'} - 3\chi^S_{x'x'y'y'z'} - 3\chi^S_{y'x'x'y'z'} + \chi^S_{y'y'y'y'z'})f_x^3 f_z + \\
&\quad + \frac{1}{8}f_z^{(4)}(\chi^S_{z'x'x'x'x'} - 6\chi^S_{z'x'x'y'y'} + \chi^S_{z'y'y'y'y'})f_x^4
\end{aligned}
$$

With 12 independent tensor elements (corresponding to 2mm symmetry):

$\chi^S_{x'x'x'x'z'}$, $\chi^S_{x'x'y'y'z'}$, $\chi^S_{x'x'z'z'z'}$, $\chi^S_{y'x'x'y'z'}$, $\chi^S_{y'y'y'y'z'}$, $\chi^S_{y'y'z'z'z'}$, $\chi^S_{z'x'x'x'x'}$, $\chi^S_{z'x'x'y'y'}$, $\chi^S_{z'x'x'z'z'}$, $\chi^S_{z'y'y'y'y'}$, $\chi^S_{z'y'y'z'z'}$, $\chi^S_{z'z'z'z'z'}$

The coefficients for the quadrupole contribution (corresponding to m3m symmetry) are very long expressions and are therefore listed in appendix E.

The tables for the $3m$ symmetry differ from those prepared by Yun-Shik Lee because a different surface coordinate system was used.

3.3.2 Angular distribution of the signal from Si(111)

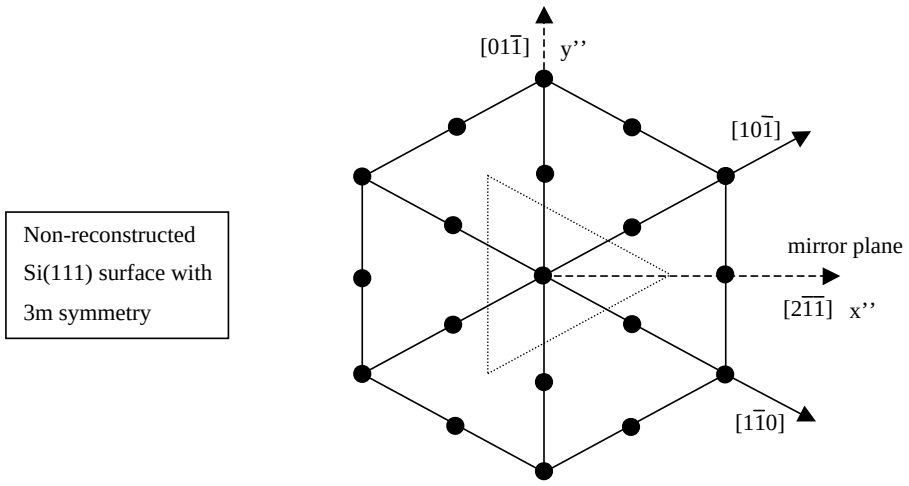

Figure 3.2: *Definition of surface coordinate system for the Si(111) surface*

Table 3.4: *SHG surface dipole (D^S) and bulk quadrupole (Q^B) contributions of Si(111)*

		Isotropic	Anisotropic (3ϕ)
S-in, S-out	D^S	0	$b^S_{SS}\sin 3\phi$
S-in, S-out	Q^B	0	$b^Q_{SS}\sin 3\phi$
S-in, P-out	D^S	a^S_{SP}	$b^S_{SP}\cos 3\phi$
S-in, P-out	Q^B	a^Q_{SP}	$b^Q_{SP}\cos 3\phi$
P-in, S-out	D^S	0	$b^S_{PS}\sin 3\phi$
P-in, S-out	Q^B	0	$b^Q_{PS}\sin 3\phi$
P-in, P-out	D^S	a^S_{PP}	$b^S_{PP}\cos 3\phi$
P-in, P-out	Q^B	a^Q_{PP}	$b^Q_{PP}\cos 3\phi$

$$
\begin{aligned}
b^S_{SS} &= f^{(2)}_y \chi^S_{x''x''x''} f^2_y \\
a^S_{SP} &= f^{(2)}_z \chi^S_{z''x''x''} f^2_y \\
b^S_{SP} &= -f^{(2)}_x \chi^S_{x''x''x''} f^2_y \\
b^S_{PS} &= -f^{(2)}_y \chi^S_{x''x''x''} f^2_x \\
a^S_{PP} &= 2f^{(2)}_x \chi^S_{x''x''z''} f_x f_z + f^{(2)}_z (\chi^S_{z''x''x''} f^2_x + \chi^S_{z''z''z''} f^2_z) \\
b^S_{PP} &= f^{(2)}_x \chi^S_{x''x''x''} f^2_x
\end{aligned}
$$

With 4 independent tensor elements (corresponding to 3m symmetry):

$\chi^S_{x''x''x''} = -\chi^S_{x''y''y''} = -\chi^S_{y''y''x''}$, $\chi^S_{x''x''z''} = \chi^S_{y''y''z''}$, $\chi^S_{z''x''x''} = \chi^S_{z''y''y''}$, $\chi^S_{z''z''z''}$

$$
\begin{aligned}
b^Q_{SS} &= \frac{\sqrt{2}}{6} f^{(2)}_y (\chi^Q_{xxxx} - \chi^Q_{xxyy} - 2\chi^Q_{xyxy}) k_z f_y^2 \\
a^Q_{SP} &= \frac{1}{6} f^{(2)}_x (\chi^Q_{xxxx} + 5\chi^Q_{xxyy} - 2\chi^Q_{xyxy}) k_x f_y^2 + \\
&\quad + \frac{1}{6} f^{(2)}_z (2\chi^Q_{xxxx} + 4\chi^Q_{xxyy} - 4\chi^Q_{xyxy}) k_z f_y^2 \\
b^Q_{SP} &= \frac{\sqrt{2}}{6} f^{(2)}_x (-\chi^Q_{xxxx} + \chi^Q_{xxyy} + 2\chi^Q_{xyxy}) k_z f_y^2 + \\
&\quad + \frac{\sqrt{2}}{6} f^{(2)}_z (-\chi^Q_{xxxx} + \chi^Q_{xxyy} + 2\chi^Q_{xyxy}) k_x f_y^2 \\
b^Q_{PS} &= -\frac{\sqrt{2}}{6} f^{(2)}_y (\chi^Q_{xxxx} - \chi^Q_{xxyy} - 2\chi^Q_{xyxy}) (k_z f_x + k_x f_z) f_x \\
a^Q_{PP} &= \frac{1}{2} f^{(2)}_x (\chi^Q_{xxxx} + \chi^Q_{xxyy} + 2\chi^Q_{xyxy}) k_x f_x^2 + \\
&\quad + \frac{2}{3} f^{(2)}_x (\chi^Q_{xxxx} - \chi^Q_{xxyy} + \chi^Q_{xyxy}) k_z f_x f_z + \\
&\quad + \frac{1}{3} f^{(2)}_x (\chi^Q_{xxxx} + 2\chi^Q_{xxyy} - 2\chi^Q_{xyxy}) k_z f_x f_z + \\
&\quad + \frac{1}{3} f^{(2)}_z (\chi^Q_{xxxx} + 2\chi^Q_{xxyy} - 2\chi^Q_{xyxy}) k_z f_x^2 + \\
&\quad + \frac{2}{3} f^{(2)}_z (\chi^Q_{xxxx} - \chi^Q_{xxyy} + \chi^Q_{xyxy}) k_x f_x f_z + \\
&\quad + \frac{1}{3} f^{(2)}_z (\chi^Q_{xxxx} + 2\chi^Q_{xxyy} + 4\chi^Q_{xyxy}) k_z f_z^2 \\
b^Q_{PP} &= \frac{\sqrt{2}}{6} f^{(2)}_x (\chi^Q_{xxxx} - \chi^Q_{xxyy} - 2\chi^Q_{xyxy}) (k_z f_x + 2k_x f_z) f_x + \\
&\quad + \frac{\sqrt{2}}{6} f^{(2)}_z (\chi^Q_{xxxx} - \chi^Q_{xxyy} - 2\chi^Q_{xyxy}) k_x f_x^2
\end{aligned}
$$

With 3 independent tensor elements (corresponding to m3m symmetry):

$\chi^Q_{xxxx} = \chi^Q_{yyyy} = \chi^Q_{zzzz}$, $\chi^Q_{xxyy} = \chi^Q_{yyzz} = \chi^Q_{yyxx} = \chi^Q_{yyzz} = \chi^Q_{zzxx} = \chi^Q_{zzyy}$, $\chi^Q_{xyxy} = \chi^Q_{xzxz} = \chi^Q_{yxxy} = \chi^Q_{yzyz} = \chi^Q_{zxxz} = \chi^Q_{zyyz}$

Table 3.5: *THG bulk dipole contributions of Si(111)*

	Isotropic	Anisotropic (3ϕ)
S-in, S-out	a_{SS}	0
S-in, P-out	0	$b_{SP}\sin 3\phi$
P-in, S-out	0	$b_{PS}\sin 3\phi$
P-in, P-out	a_{PP}	$b_{PP}\cos 3\phi$

$$
\begin{aligned}
a_{SS} &= \frac{1}{2} f_y^{(3)} (\chi_{xxxx} + 3\chi_{xxyy}) f_y^3 \\
b_{SP} &= \frac{\sqrt{2}}{6} f_z^{(3)} (\chi_{xxxx} - 3\chi_{xxyy}) f_y^3 \\
b_{PS} &= -\frac{1}{\sqrt{2}} f_y^{(3)} (\chi_{xxxx} - 3\chi_{xxyy}) f_x^2 f_z \\
a_{PP} &= \frac{1}{2} f_x^{(3)} ((\chi_{xxxx} + 3\chi_{xxyy}) f_x^2 + 2\chi_{xxxx} f_z^2) f_x + \\
&\quad + \frac{1}{3} f_z^{(3)} (3\chi_{xxxx} f_x^2 + (\chi_{xxxx} + 6\chi_{xxyy}) f_z^2) f_z \\
b_{PP} &= \frac{1}{\sqrt{2}} f_x^{(3)} (\chi_{xxxx} - 3\chi_{xxyy}) f_x^2 f_z + \\
&\quad + \frac{\sqrt{2}}{6} f_z^{(3)} (\chi_{xxxx} - 3\chi_{xxyy}) f_x^3
\end{aligned}
$$

With 2 independent tensor elements (corresponding to m3m symmetry):

$\chi_{xxxx} = \chi_{yyyy} = \chi_{zzzz}$

$\chi_{xxyy} = \chi_{xxzz} = \chi_{yyxx} = \chi_{yyzz} = \chi_{zzxx} = \chi_{zzyy}$

Table 3.6: *FHG surface dipole (D^S) and bulk quadrupole (Q^B) contributions of Si(111)*

		Isotropic	Anisotropic (3ϕ)	Anisotropic (6ϕ)
S-in, S-out	D^S	0	$b^S_{SS}\sin 3\phi$	0
S-in, S-out	Q^B	0	$b^Q_{SS}\sin 3\phi$	$c^Q_{PP}\sin 6\phi$
S-in, P-out	D^S	a^S_{SP}	$b^S_{SP}\cos 3\phi$	0
S-in, P-out	Q^B	a^Q_{SP}	$b^Q_{SP}\cos 3\phi$	$c^Q_{SP}\cos 6\phi$
P-in, S-out	D^S	0	$b^S_{PS}\sin 3\phi$	0
P-in, S-out	Q^B	0	$b^Q_{PS}\sin 3\phi$	$c^Q_{PS}\sin 6\phi$
P-in, P-out	D^S	a^S_{PP}	$b^S_{PP}\cos 3\phi$	0
P-in, P-out	Q^B	a^Q_{PP}	$b^Q_{PP}\cos 3\phi$	$c^Q_{PP}\cos 6\phi$

$$
\begin{aligned}
b_{SS} &= f_y^{(4)}\chi^S_{x''x''x''x''x''x''}f_y^4 \\
a_{SP} &= -f_x^{(4)}(\chi^S_{x''x''x''x''x''x''}+2\chi^S_{x''x''x''y''y''}f_y^4 \\
b_{SP} &= f_z^{(4)}\chi^S_{z''x''x''x''x''x''}f_y^4 \\
b_{PS} &= -f_y^{(4)}(\chi^S_{x''x''x''x''x''}f_x^2+2\chi^S_{x''x''x''y''y''}f_x^2+6\chi^S_{x''x''x''z''z''}f_z^2)f_x^2 \\
a_{PP} &= 4f_x^{(4)}(\chi^S_{x''x''x''x''z''}f_x^3f_z+\chi^S_{x''x''z''z''z''}f_xf_z^3)+ \\
&\quad +f_z^{(4)}(\chi^S_{z''x''x''x''x''}f_x^4+6\chi^S_{z''x''x''z''z''}f_x^2f_z^2+\chi^S_{z''z''z''z''z''}f_z^4) \\
b_{PP} &= f_x^{(4)}(\chi^S_{x''x''x''x''x''}f_x^4+6\chi^S_{x''x''x''z''z''}f_x^2f_z^2)+4f_z^{(4)}\chi^S_{z''x''x''x''z''}f_x^3f_z
\end{aligned}
$$

With 7 independent tensor elements (corresponding to 3m symmetry):

$\chi^S_{x''x''x''x''x''}$, $\chi^S_{x''x''x''x''z''}=3\chi^S_{x''x''y''y''z''}=3\chi^S_{y''x''x''y''z''}=\chi^S_{y''z''y''y''y''}$, $\chi^S_{x''x''x''y''y''}$, $\chi^S_{x''x''x''z''z''}=-\chi^S_{x''y''y''z''z''}$, $\chi^S_{x''x''z''z''z''}=\chi^S_{y''y''z''z''z''}$, $\chi^S_{z''x''x''x''x''}=3\chi^S_{z''x''x''y''y''}=\chi^S_{z''y''y''y''y''}$, $\chi^S_{z''x''x''x''z''}=-\chi^S_{z''x''y''y''z''}$, $\chi^S_{z''x''x''z''z''}=\chi^S_{z''y''y''z''z''}$, $\chi^S_{z''z''z''z''z''}$

The following non-zero tensor elements can be expressed as linear combinations of the above independent elements

$\chi^S_{x''y''y''y''} = -\chi^S_{x''x''x''x''} - 2\chi^S_{x''x''y''y''}$, $\chi^S_{y''x''x''x''} = -\frac{1}{2}\chi^S_{x''x''x''x''} - \frac{3}{2}\chi^S_{x''x''y''y''}$,

$\chi^S_{y''x''y''y''} = -\chi^S_{x''x''x''x''} + \frac{1}{2}\chi^S_{x''x''x''y''}$

The coefficients for the quadrupole contribution (corresponding to m3m symmetry) are very long expressions and are therefore listed in appendix E.

Chapter 4

Experiments

4.1 Setup

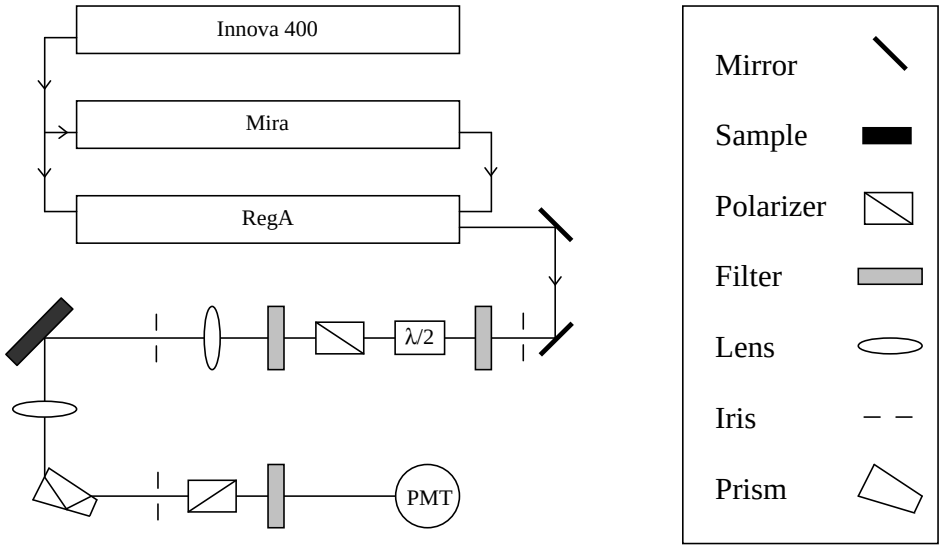

Figure 4.1: *Experimental Setup*

The laser light source used in these experiments consists of three stages. An Ar^+-ion laser (Innova 400, Coherent) provides a 24 W continuous wave pump beam in multi-visible mode. The beam enters a Ti:sapphire laser (Mira 900-B, Coherent) that can be passively mode locked and gives 120 fs pulses at a repetition rate of 78 MHz. These pulses then enter a regenerative amplifier (RegA, Coherent). An

acousto-optical modulator (AOM) inside the RegA is used to insert the pulses from Mira into the amplifier cavity. The pulse travels about 24 round trips each time passing through a titanium doped sapphire crystal, which is pumped by the Ar^+-ion laser. During the 24 cycles the pulse is stretched as it passes through the AOM. After the pulse is ejected via the AOM, it passes through an optical isolator and a four pass compressor. The system generates 200 fs pulses at a repetition rate of 250 kHz and an energy of up to $5\mu J$ per pulse. Pulses from both Mira and RegA are monitored by an autocorrelator.

When the pulses enter the experimental setup they pass an adjustable neutral density filter which adjusts the input power. With a half-wave plate and a cube polarizer the polarization state can be defined as well. After passing a red glass filter, to eliminate possible SHG from the optics, the beam is focused down onto the sample by a 35-cm focal lens. The optical response of the sample (reflected fundamental, SH, TH, FH) emerges collinearly. The beam is then re-collimated again by a second lens with a focal length of $5cm$. Then the frequency components are spatially separated using a Pellin-Broca prism that is placed on a rotational stage so that different harmonic signals can be chosen. The polarization is analyzed using a Rochon prism. The signal then passes the appropriate filters and is detected by a photon counter PMT.

4.2 Alignment

The daily alignment procedure for the laser system can be found in the appropriate Coherent manuals. Irises are included in the setup to reproduce the beam from day to day.

When the sample is changed, the orientation of the new sample with respect to the rotational axis must be aligned precisely, otherwise the reflected beam wanders while the sample is rotated which then causes an unwanted azimuthal dependence of the signal. The alignment procedure used here is as follows:

- Insert a mirror between sample and re-collimating lens.
- Close the iris directly in front of the sample to select only a small part of the beam.
- Monitor the reflected beam on a white card, at low intensities an IR-viewer useful. For fine adjustment one can use a sheet of paper attached to the wall ($\sim$ 2 meters away) as a monitor.
- Mark the initial position on the card/paper.
- Rotate the sample by 180°.
- Use the tilting screws at the sample holder to steer the reflected at a point midway between the initial and final positions.
- Repeat the last three points until the spot only moves up and down.
- Since the resolution is better in the left-right direction than in up-down, it is best to rotate the sample by 90° and use the card again.
- Set sample holder again to the initial position.

If a different harmonic signal is selected, it is necessary to rotate the Pellin-Broca prism. For proper alignment the reflected beam should be perpendicular to

the incident beam (Fig.(4.2)). A trigonometric analysis reveals that the angle of incidence α should satisfy the following condition:

$$\sin\alpha = n\sin\beta = n\sin(\delta - 45^\circ) \tag{4.1}$$

For $\delta = 79.5^\circ$ we obtain the following incident angles:

λ	$n(\omega)$	$\alpha(\omega)$
$800nm$	1.45332	55.40°
$400nm$	1.47012	56.38°
$266nm$	1.49968	58.15°
$200nm$	1.55051	61.42°

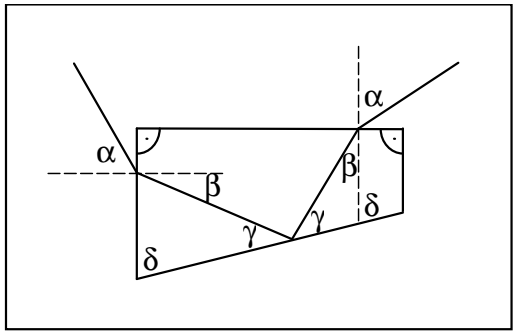

Figure 4.2: *Schematic of the beam path through the Pellin Broca prism*

Since each harmonic signal exits the prism at different spots, adjustment with a translational stage is sometimes necessary to direct the beam into the PMT, especially when changing to or from fourth harmonic measurements. Fine adjustments can be made by monitoring the count rates on the PMT while rotating and moving the prism slightly. To find the second harmonic signal it is convenient to use a frequency doubler such as $LiNbO_3$ in transmission to track the strong signal.

Since the angular dependence and the signal level are sometimes extremely

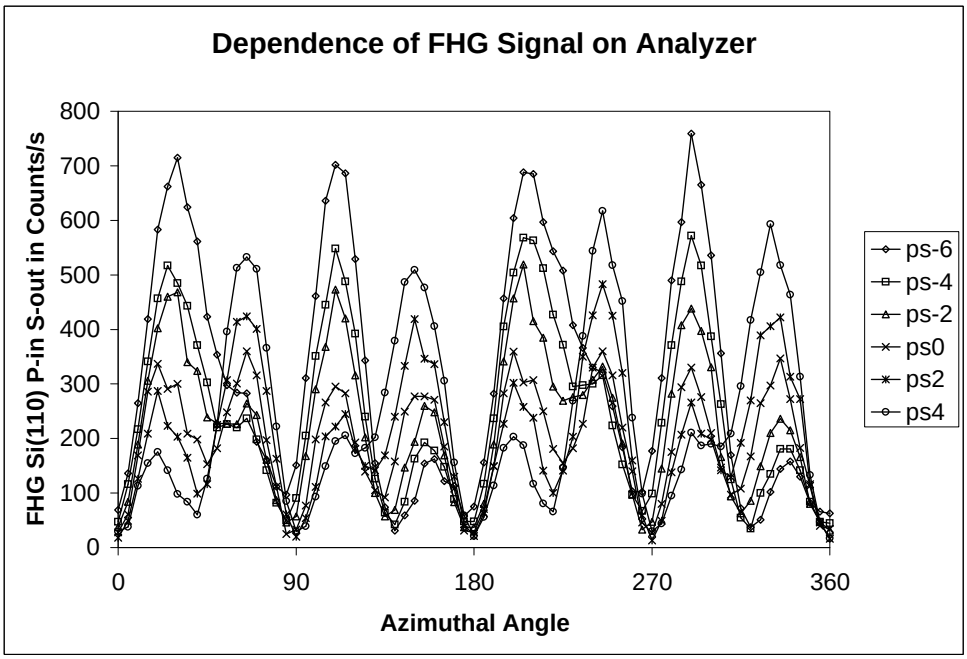

Figure 4.3: *Dependence of the FHG signal from Si(110) in P-in, S-out configuration on the position of the analyzer; ps-6 is* 6° *from the optimal position*

sensitive to the chosen polarization (Fig.(4.3), Fig.(4.4)) it is important to check the polarizer orientation by the following:

- Insert a microscope slide directly behind the polarizer.
- Adjust until the reflected light travels back along the direction of the incident beam.
- Rotate the glass slide around an axis perpendicular to the table and look for a minimum of the reflected light. The position should then be near the Brewster angle.
- Rotate the polarizer and glass slide until the reflected light vanishes.
- The beam is now fully p-polarized.

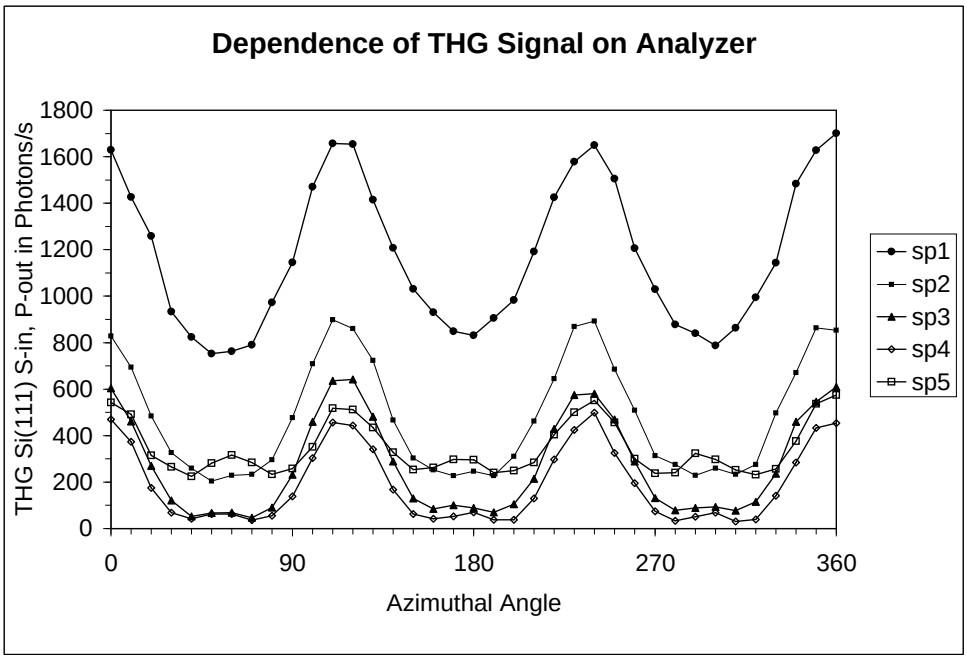

Figure 4.4: *Dependence of the THG signal from Si(110) in P-in, S-out configuration on the position of the analyzer; between each measurement the analyzer was rotated by* 1°.

4.3 Data Processing

4.3.1 Dark Counts

The dark counts were in all cases extremely low, therefore it was not necessary to subtract this contribution from the data. For FHG the dark counts were as low as 1 photon in 10 seconds.

4.3.2 Correction for high count rates

All count rates were treated with a correction formula. But only at high count rates the treatment made a difference. High count rates were accounted for in the signal by the following. The photon counting PMT only detects *if* a photon arrives

within the 200 fs of a pulse, but it cannot resolve *how many* photons arrive. If the count rate is low, only a few photon reach the PMT and so it is unlikely that more than one photon arrives within one pulse duration. When the count rate is higher the probability of more photons per count is also higher, but they are not counted separately. However, the number of counts is related to the number of detected photons.

When the pulse hits the sample each of the n electrons has a probability p to create a higher harmonic photon that reaches the PMT. Using $q = 1 - p$ the expectation value r of the number of radiation events per pulse is simply given by:

$$r = np = n(1 - q) \tag{4.2}$$

The probability c that the PMT counts a photon is simply 1 minus the probability of no count. With q from Eq.(4.2) we get:

$$c = 1 - q^n = 1 - \left(1 - \frac{r}{n}\right)^n \tag{4.3}$$

If we assume the number of electrons to be large ($n \to \infty$) we obtain:

$$c = 1 - e^{-r} \tag{4.4}$$

After solving the equation for r the final relation between the probability of a count and the actual expectation value of the radiation events is given as:

$$r = -\ln(1 - c) \tag{4.5}$$

If we measure the signal of N pulses the actual count rate is $C = Nc$ and the actual radiation events are $R = Nr$. When we insert these quantities in Eq.(4.5) and solve for R, we obtain the correction formula for the radiation events:

$$R = -N \ln\left(1 - \frac{C}{N}\right) \tag{4.6}$$

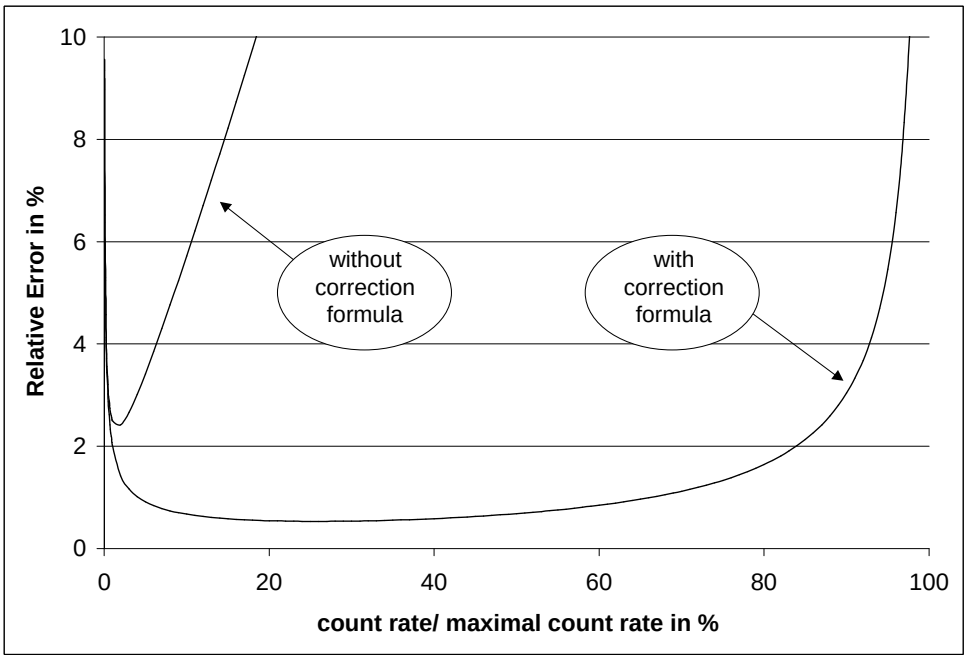

Figure 4.5: *Relative errors in R with and without correction formula for a maximal count rate* $N = 250000$ *and* $\Delta N/N = 1\%$.

By using this formula, systematic errors at high count rates can be eliminated. Fig.(4.5) shows the total error[1] that accumulates when the correction formula is used in comparison to the statistical and systematic errors that occur when the correction formula is not used.

4.3.3 Detector Efficiency

In order to relate the number of counts to the size of the susceptibility an analysis of the detector efficiency as well as a measurement of the pulse duration and peak intensity was necessary.

[1] Statistical error $\sqrt{R}^{(-1)}$ and error due to variation of maximal count rate N

After the higher harmonics are generated the beam passes through a re-collimating lens, a Pellin Broca prism, a Rochon Prism and filters before finally reaching a PMT that can be described by a certain quantum efficiency. The estimated transmittance is summarized in the following table:

	SHG	THG	FHG
lens	93 %	92 %	91 %
Pellin Broca prism (s-pol.)	74 %	70 %	63 %
Pellin Broca prism (p-pol.)	65 %	61 %	55 %
Rochon polarizer	93 %	92 %	91 %
filter	80 %	13 %	17 %
PMT	25 %	25 %	16 %
total (s-polarized)	13 %	1.9 %	1.4 %
total (p-polarized)	11 %	1.7 %	1.2 %

4.3.4 Beam Characterization

As mentioned in the introduction, the higher harmonic generation depends strongly on the incident electric peak intensity and the pulse duration.

The *pulse duration* can be measured by autocorrelation where the setup is commonly known as a Michelson interferometer. While one mirror of an interferometer stays fixed the other is moved by microns. The recombined beams are focused onto a frequency doubler crystal (KDP) and the generated SH signal is measured by a PMT. Fig.(4.6) shows the result. The data were fit with a Lorentzian. To determine the pulse duration of the deconvoluted pulse it was necessary to halve the FWHM of the autocorrelation function. The pulse duration obtained is $\tau = 200fs$.

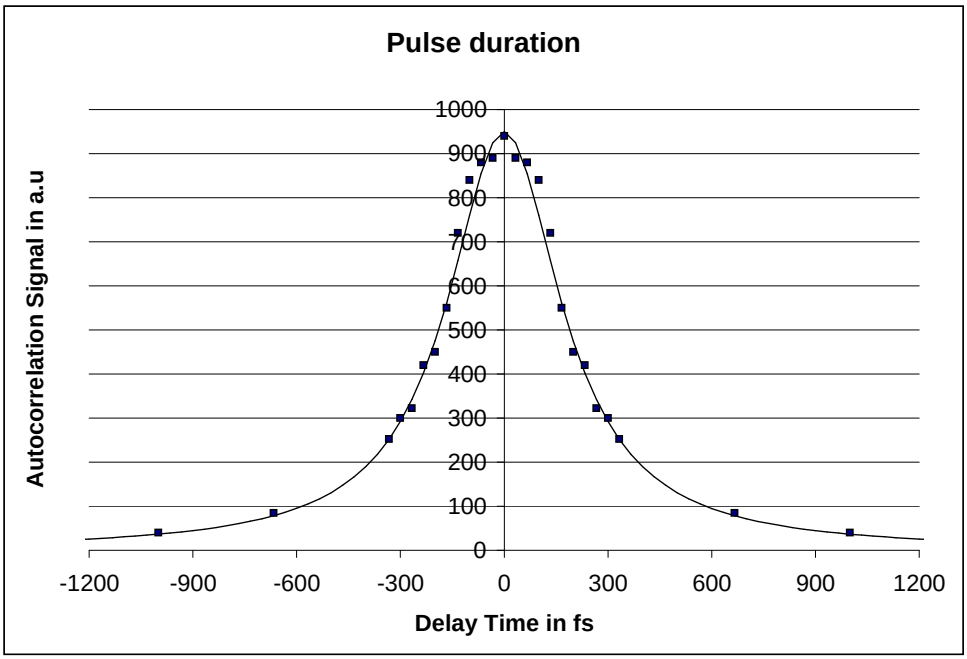

Figure 4.6: *Measurement to determine the pulse duration*

4.4 Checks for Fourth Harmonic Signal

4.4.1 Power dependence of fourth harmonic signals and determination of damage threshold

As discussed earlier the fourth harmonic signal scales as the fourth power of the incident power. Fig.(4.7) shows the power dependence of the FH from Si(111) in the P-in, P-out configuration. The fit curve has a slope of 4, indicating the 'cleanness' of the signal.

The deviation of the data from the curve at higher incident powers can be explained. The FHG signal from Si(111) is mainly generated at the surface. At a certain level of incident power the surface is damaged and the signal drops. Since the value of the damage occurs at flux rates of about $0.1\frac{J}{cm^2}$ which corresponds to a damage intensity of $5 \cdot 10^{-11}\frac{W}{cm^2}$, we can calibrate the data.

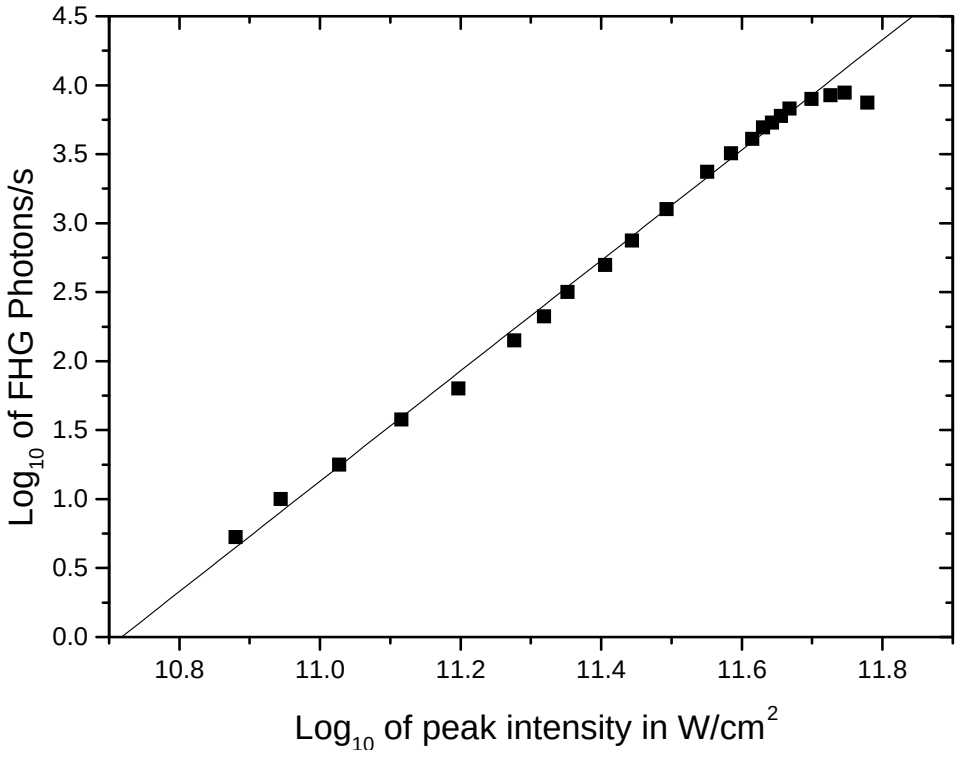

Figure 4.7: *Intensity dependence of FHG for Si(111), P-in, P-out configuration*

4.4.2 Leakage of other Harmonics

Finally, it is important to consider whether non-fourth harmonic contributions have leaked into the signal. After a proper alignment for FHG measurements the azimuthal dependence of non-fourth harmonic components were measured by placing additional filters for the appropriate wavelengths of fundamental, SH and TH between the Pellin-Broca prism and the fourth harmonic bandpass filter. Fig.(4.8) shows the results. The nearly zero counts for the fundamental and second harmonic light proves the absence of these contributions. Using the additional THG filter the counts match very well with the 2% transmittance of FHG by the TH filter. Therefore, leakage of other non-fourth harmonic components into the signal is not

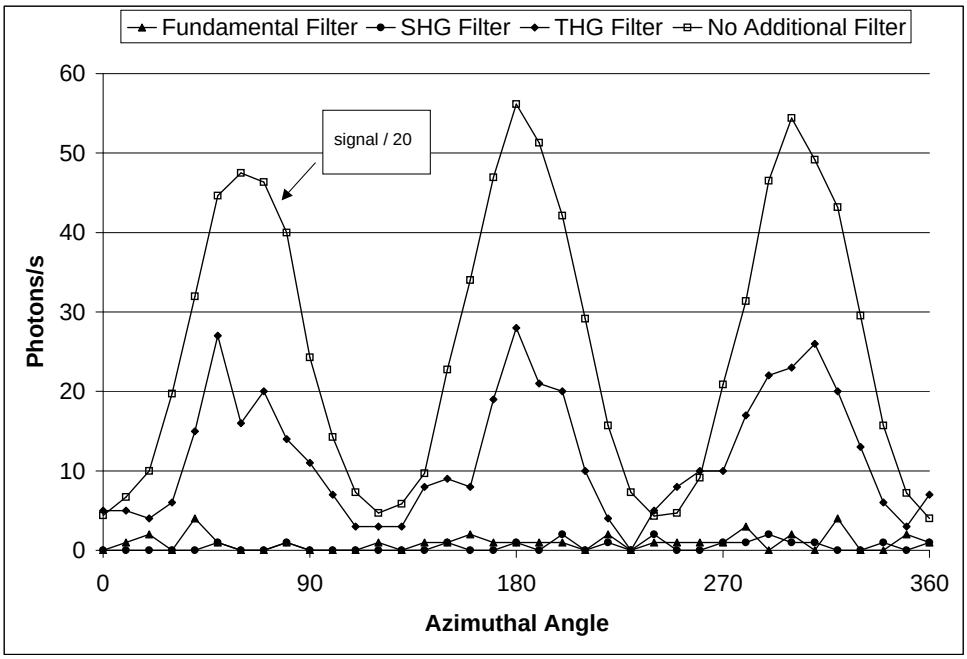

Figure 4.8: *Measurement of possible leakage of other frequencies to the FHG signal*

occurring.

4.5 Study of Si(110) Surface

4.5.1 Second Harmonic Signal

The SHG signals from Si(110) presented in Figs. [4.9] thru [4.12] are fitted in terms of surface dipole, DC-induced and quadrupole polarizations (see Table 3.1). The additional four-fold anisotropic quadrupole terms are necessary to fit the plateaus in the P-in, P-out and S-in, S-out signal. With this terms the χ^2-value could be lowered by a factor of 0.5. The best fits for not included bulk quadrupole terms are indicated by gray lines in the graphs. In addition the four peaks in the P-in, S-out configuration seem to be unequally spaced which indicates also a four-fold contribution in the polarization. However, the signal is not as clean in this

configuration. Therefore the possible four-fold polarization contribution has a high uncertainty and the phase shift between two-fold and four-fold contribution to the polarization could not be determined in this case. The high counts in S-in, S-out configuration originate from damaged spots on the sample. To obtain the errors in the fit parameters they were changed slightly until the deviation of the resulting curve from the fit curve was not acceptable any more.

The used fit functions are:

P-in, P-out: $|a_{pp}e^{i\alpha} + b_{pp}e^{i\beta}\cos(2\phi) + c_{pp}\cos(4\phi)|^2$

where $a_{pp}e^{i\alpha} = a^S_{pp} + a^Q_{pp}$, $b_{pp}e^{i\beta} = b^S_{pp} + b^Q_{pp}$, $c_{pp} = c^Q_{pp}$

$a_{pp} = 129 \pm 2, b_{pp} = 36 \pm 4, c_{pp} = 7.0 \pm 3, \alpha = 142° \pm 60°, \beta = 110° \pm 50°$

P-in, S-out: $|b_{ps}e^{i\beta}\sin(2\phi) + c_{ps}\sin(4\phi)|^2$

where $b_{ps}e^{i\beta} = b^S_{ps} + b^Q_{ps}$, $c_{ps} = c^Q_{ps}$

$b_{ps} = 37 \pm 2, c_{ps} = 3 \pm 9, \beta = 300° \pm 360°$

S-in, P-out: $|a_{sp}e^{i\alpha} + b_{sp}e^{i\beta}\cos(2\phi) + c_{sp}\cos(4\phi)|^2$

where $a_{sp}e^{i\alpha} = a^S_{sp} + a^Q_{sp}$, $b_{sp}e^{i\beta} = b^S_{sp} + b^Q_{sp}$, $c_{sp} = c^Q_{sp}$

$a_{sp} = 62.5 \pm 3, b_{sp} = 17.4 \pm 3, c_{sp} = 3.2 \pm 2, \alpha = 209° \pm 50°, \beta = 12° \pm 35°$

S-in, S-out: 0

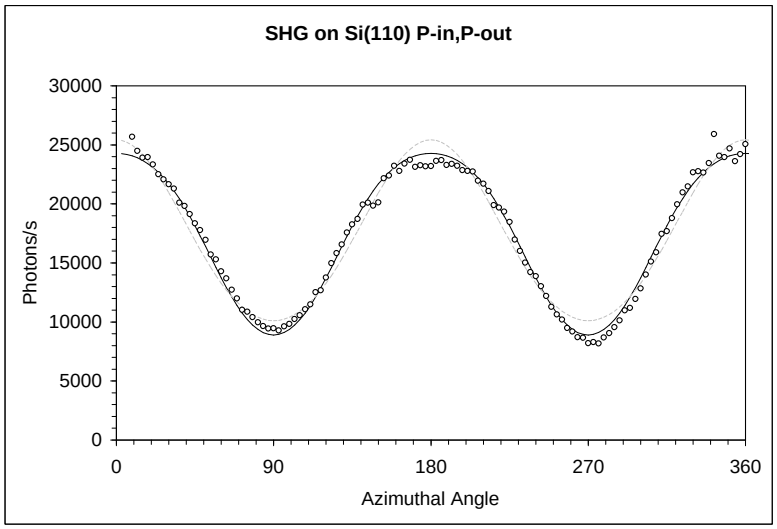

Figure 4.9: *SHG from Si(110) in P-in, P-out configuration at input power of 40mW*

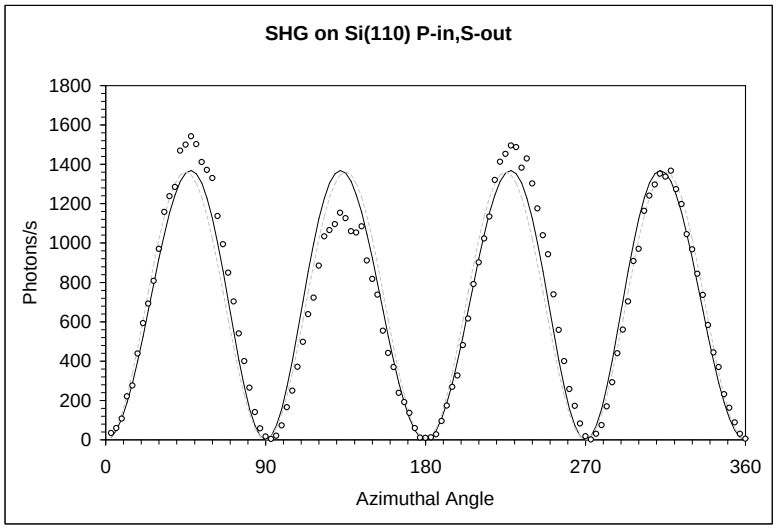

Figure 4.10: *SHG from Si(110) in P-in, S-out configuration at input power of 40mW*

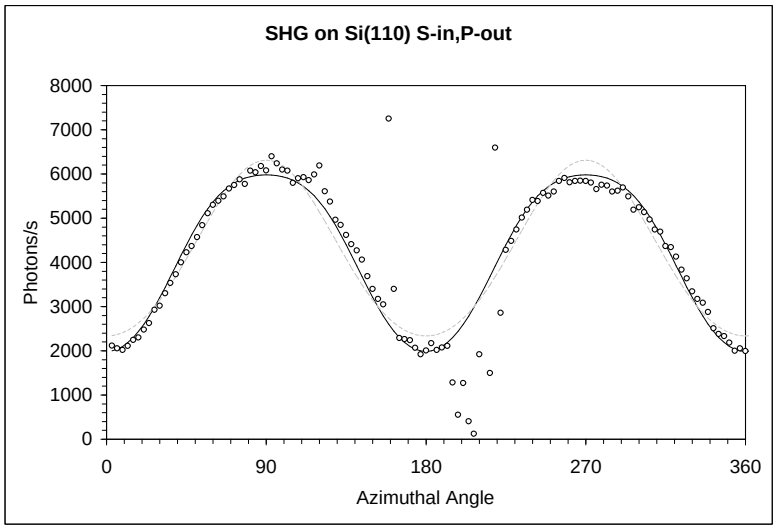

Figure 4.11: *SHG from Si(110) in S-in, P-out configuration at input power of 40mW*

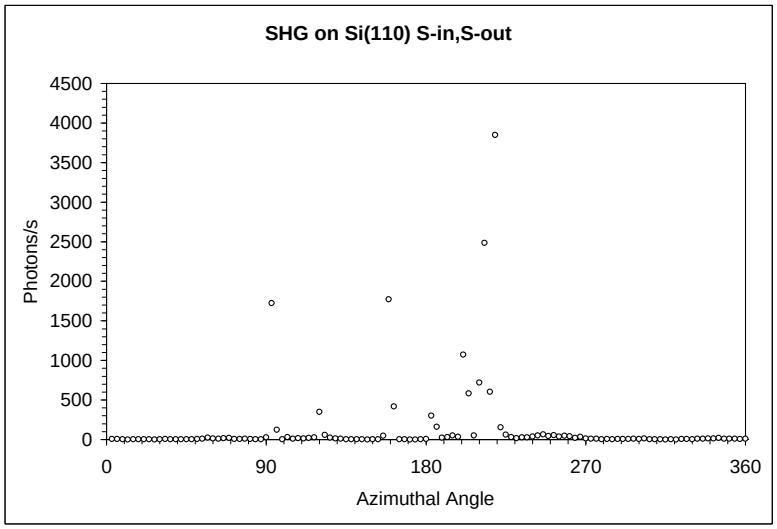

Figure 4.12: *SHG from Si(110) in S-in, S-out configuration at input power of 40mW*

4.5.2 Third Harmonic Signal

The THG signal from Si(110) presented in Figs. [4.13] thru [4.16] is well described by the dipole bulk polarization. It is extremely hard to isolate the P-in, S-out and S-in, P-out configurations as the signal levels of P-in, P-out and S-in, S-out are 600 and 60 times higher, respectively. If the analyzer is not aligned within fractions of a degree the leakage for this high (PP and SS) signals obscure the signal of PS and SP. As a large signal the leakage from PP is more severe. But in to case of the PS configuration the nearly s-polarized electric field contributes to the interaction with its third power and therefore the effect of the small fraction of p-polarized light is suppressed. Nevertheless it is not possible to fit the azimuthal dependence of the third harmonic signal in SP configuration satisfactorily, but it still gives an indication about the relative size of the signal.

The used fit functions are:

P-in, P-out: $|a_{pp}e^{i\alpha} + b_{pp}e^{i\beta}\cos(2\phi) + c_{pp}\cos(4\phi)|^2$

$a_{pp} = 147 \pm 3, b_{pp} = 24 \pm 4, c_{pp} = 12.5 \pm 3, \alpha = 194° \pm 8°, \beta = 330° \pm 15°$

P-in, S-out: $|b_{ps}e^{i\beta}\sin(2\phi) + c_{ps}\sin(4\phi)|^2$

$b_{ps} = 4.4 \pm 0.3, c_{ps} = 8.8 \pm 0.4, \beta = 0° \pm 40°$

S-in, P-out: $|b_{sp}e^{i\beta}\sin(2\phi) + c_{sp}\sin(4\phi)|^2$

$b_{ps} = 5.5 \pm 3, c_{ps} = 7 \pm 2, \beta = 145° \pm 360°$

S-in, S-out: $|a_{ss}e^{i\alpha} + b_{ss}e^{i\beta}\cos(2\phi) + c_{ss}\cos(4\phi)|^2$

$a_{pp} = 49 \pm 1, b_{pp} = 9.3 \pm 2, c_{pp} = 4.3 \pm 1, \alpha = 163° \pm 8°, \beta = 212° \pm 10°$

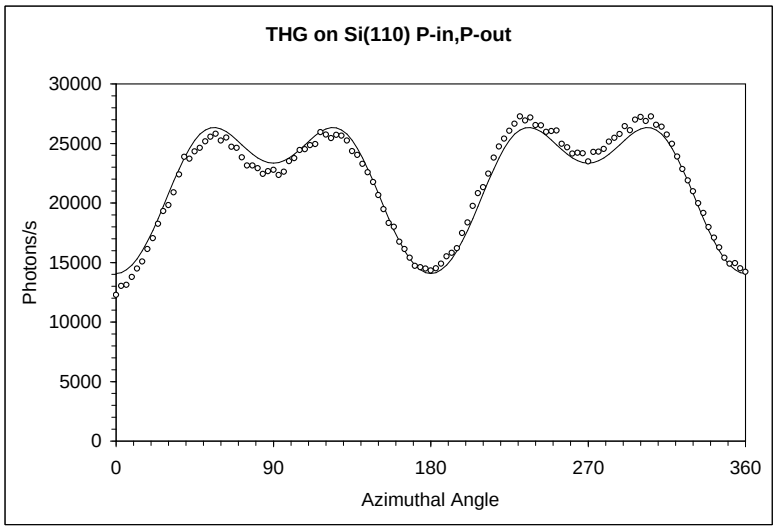

Figure 4.13: *THG from Si(110) in P-in, P-out configuration at input power of 6mW*

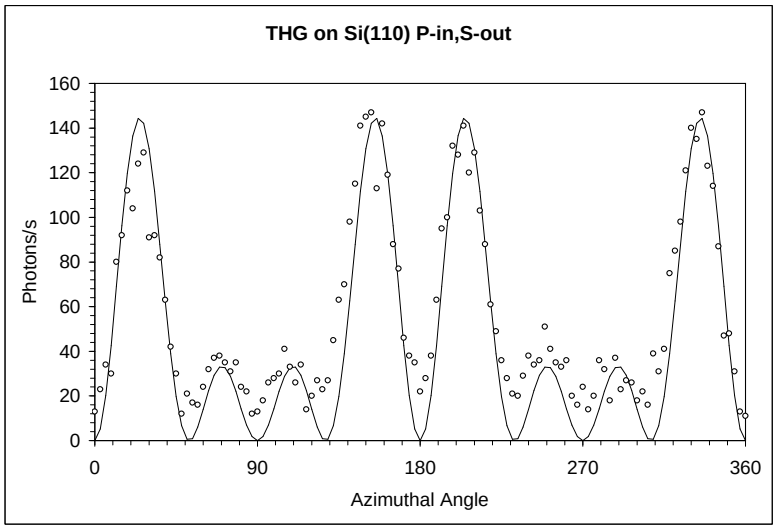

Figure 4.14: *THG from Si(110) in P-in, S-out configuration at input power of 6mW*

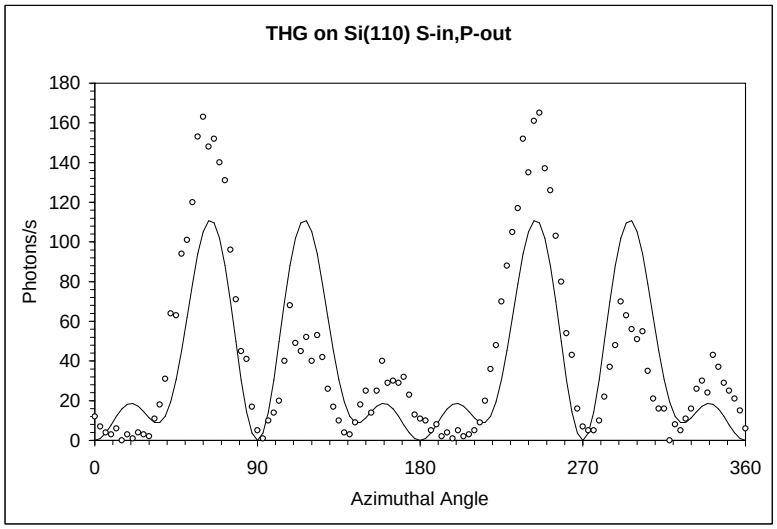

Figure 4.15: *THG from Si(110) in S-in, P-out configuration at input power of 6mW*

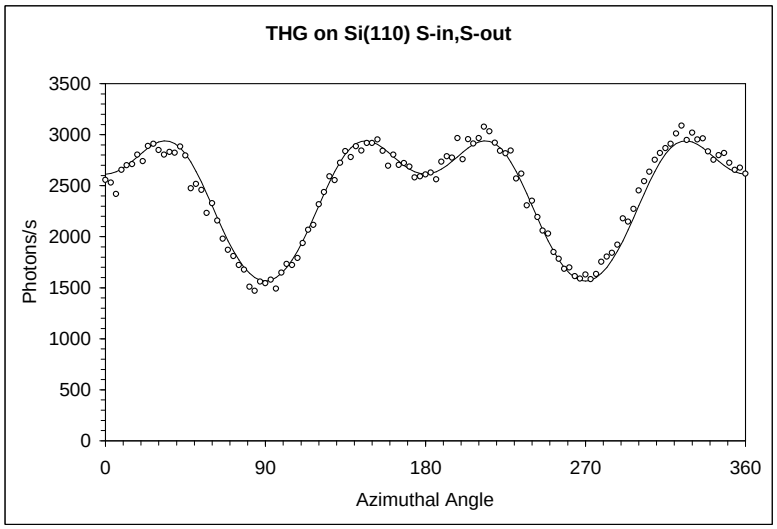

Figure 4.16: *THG from Si(110) in S-in, S-out configuration at input power of 6mW*

4.5.3 Fourth Harmonic Signal

The FHG signal from Si(110) presented in Figs. [4.17] thru [4.20]. The signal is relatively strong in P-in, P-out configuration and has a reliable azimuthal dependence. It signal is well described by the surface dipole polarization and DC induced polarization. Only in the S-in, P-out configuration the additional term proportional to $\cos(6\phi)$ that originates from the quadrupole polarization improved the fit curves significantly and reshaped sharper peaks. Even with an hypothetic offset this peaks could not be fit just by dipole terms. Due to the low intensity and the small number of counts in this configuration this measurement gives only an indication of the importance of the bulk quadrupole contribution for fourth harmonic generation. The isotropic counts in S-in, S-out configuration are far above the level of stray light in the room as the dark count rate for this experiment was approximately 1 count in 10 s. This experiment was repeated after cleaning the surface with acetone to check whether these counts originate from surface termination but no change was detected. A possible source could be a rough Si/SiO_2 interface which was not removed by the cleaning. One way to check this assumption would be to create additional roughness by etching the surface. A more convincing way would be to remove the oxide layer, anneal the sample and take the measurements under UV-conditions.

The used fit functions are:

P-in, P-out: $|a_{pp}e^{i\alpha} + b_{pp}e^{i\beta}\cos(2\phi) + c_{pp}\cos(4\phi)|^2$

where $a_{pp}e^{i\alpha} = a^S_{pp} + a^Q_{pp}$, $b_{pp}e^{i\beta} = b^S_{pp} + b^Q_{pp}$, $c_{pp} = c^S_{pp} + c^Q_{pp}$

$a_{pp} = 35.4 \pm 0.6, b_{pp} = 15.8 \pm 1.0, c_{pp} = 11.0 \pm 1.3, \alpha = 342° \pm 5°, \beta = 157° \pm 5°$

P-in, S-out: $|b_{ps}e^{i\beta}\sin(2\phi) + b_{ps}\sin(4\phi)|^2$

where $b_{ps}e^{i\beta} = b_{ps}^S + b_{ps}^Q$, $c_{ps} = b_{ps}^S + c_{ps}^Q$

$a_{ps} = 4.1 \pm 0.8, b_{ps} = 6.2 \pm 0.6, \beta = 90^\circ \pm 5^\circ$

S-in, P-out: $|a_{sp}e^{i\alpha} + b_{sp}e^{i\beta}\cos(2\phi) + c_{sp}e^{i\gamma}\cos(4\phi) + d_{sp}\cos(6\phi)|^2$

where $a_{sp}e^{i\alpha} = a_{sp}^S + a_{sp}^Q$, $b_{sp}e^{i\beta} = b_{sp}^S + b_{sp}^Q$, $c_{sp}e^{i\gamma} = c_{sp}^S + c_{sp}^Q$, $d_{sp} = d_{sp}^Q$

$a_{sp} = 4.36 \pm 0.12, b_{sp} = 1.8 \pm 0.3, c_{sp} = 0.4 \pm 0.4, d_{sp} = 0.63 \pm 0.38, \alpha = 332^\circ \pm 30^\circ, \beta = 188^\circ \pm 30^\circ, \gamma = 86^\circ \pm 30^\circ$

P-in, S-out: 0

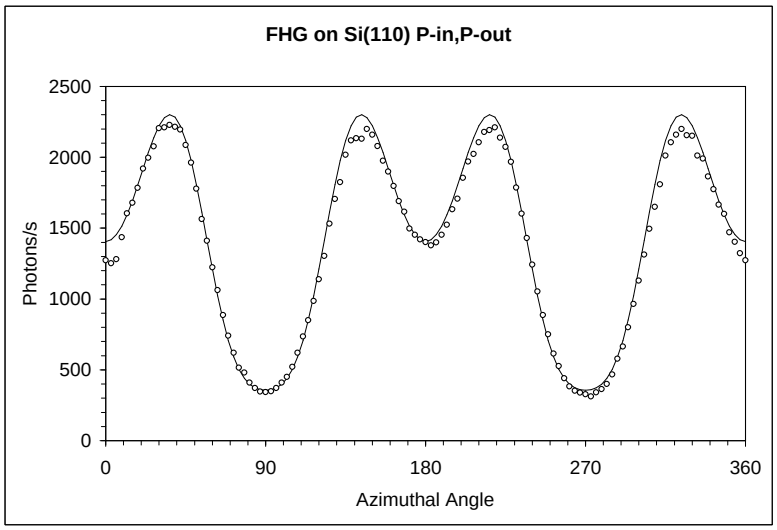

Figure 4.17: *FHG from Si(110) in P-in, P-out configuration at input power of 350mW*

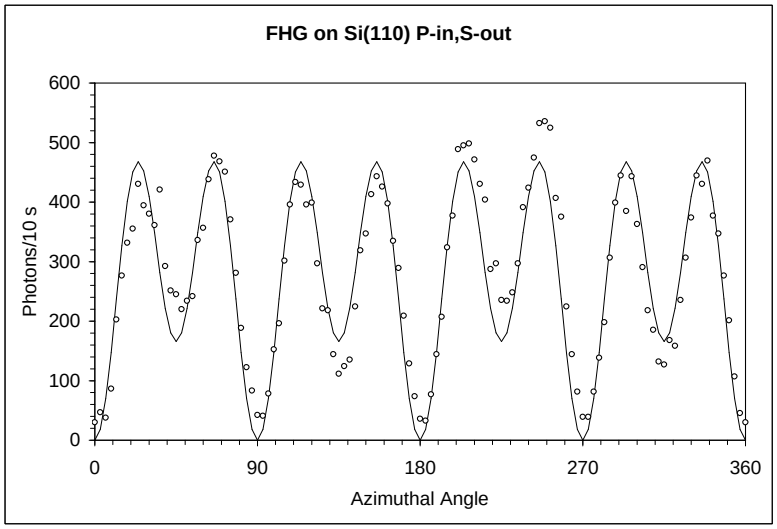

Figure 4.18: *FHG from Si(110) in P-in, S-out configuration at input power of 350mW*

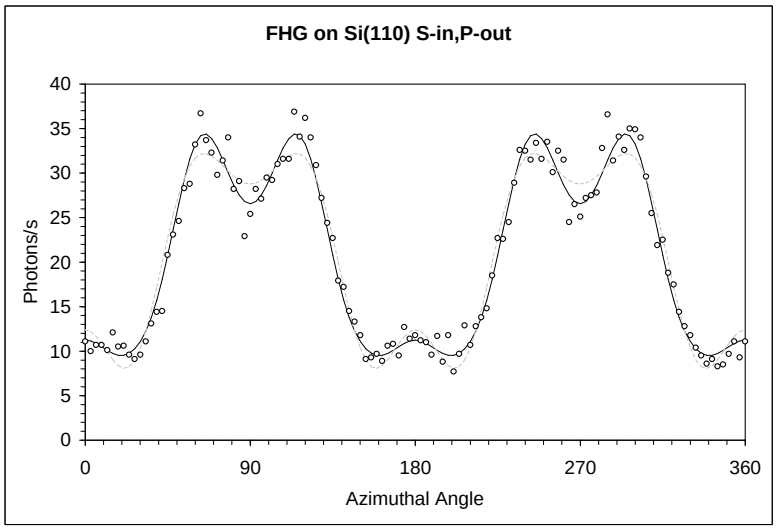

Figure 4.19: *FHG from Si(110) in S-in, P-out configuration at input power of 350mW*

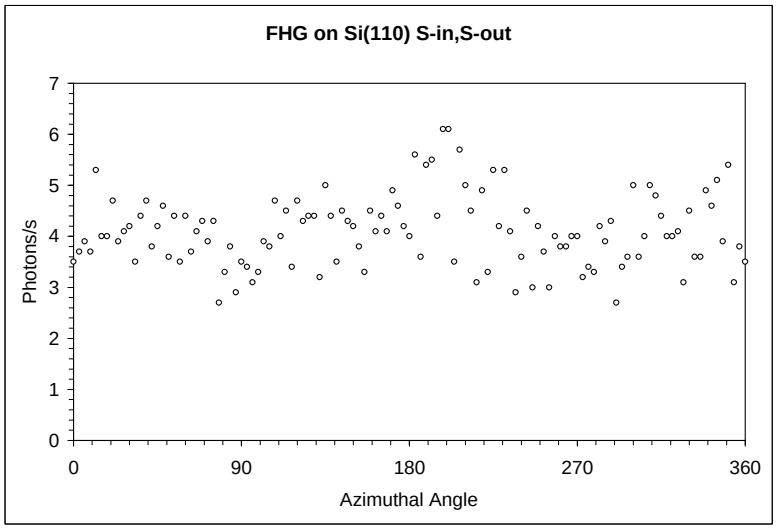

Figure 4.20: *FHG from Si(110) in S-in, S-out configuration at input power of 350mW*

4.6 Study of Si(111) Surface

4.6.1 Second Harmonic Signal

The azimuthal dependence of the SHG signal from Si(111) is shown in Figs. [4.21] thru [4.24]. In all polarization configurations the derived functions with maximal three free parameters fit the data excellent. It is impossible to distinguish the contributions form the surface dipole and bulk quadrupole tensor (see Table 3.4).

The fit functions are:

P-in, P-out: $|a_{pp}e^{i\alpha} + b_{pp}\cos(3\phi)|^2$

where $a_{pp}e^{i\alpha} = a^S_{pp} + a^Q_{pp}$, $b_{pp} = b^S_{pp} + b^Q_{pp}$

$a_{pp} = 162 \pm 5, b_{pp} = 208 \pm 6, \alpha = 144^\circ \pm 2^\circ$

P-in, S-out: $|b_{ps}\sin(3\phi)|^2$

where $b_{ps} = b^S_{ps} + b^Q_{ps}$

$b_{ps} = 148 \pm 3$

S-in, P-out: $|a_{sp}e^{i\alpha} + b_{sp}\cos(3\phi)|^2$

where $a_{sp}e^{i\alpha} = a^S_{sp} + a^Q_{sp}$, $b_{sp} = b^S_{sp} + b^Q_{sp}$

$a_{sp} = 81.2 \pm 4, b_{sp} = 98.4 \pm 4, \alpha = 133^\circ \pm 3^\circ$

S-in, S-out: $|b_{ss}\sin(3\phi)|^2$

where $b_{ss} = b^S_{ss} + b^Q_{ss}$

$b_{ss} = 79 \pm 4$

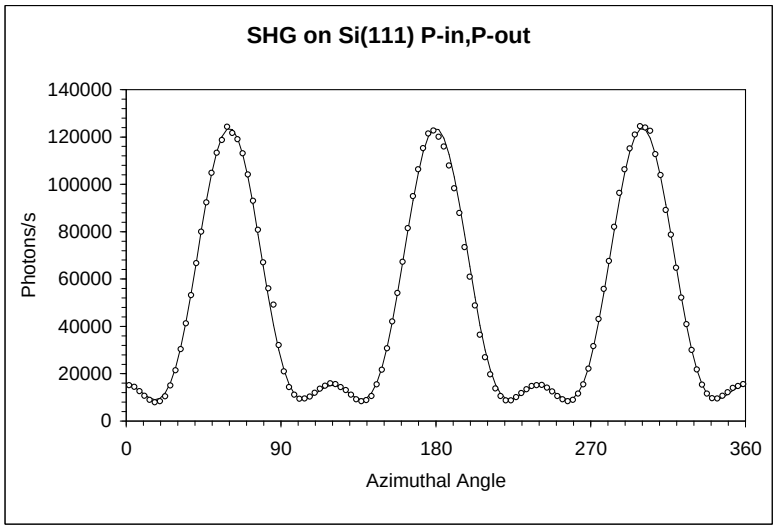

Figure 4.21: *SHG from Si(111) in P-in, P-out configuration at input power of 40mW*

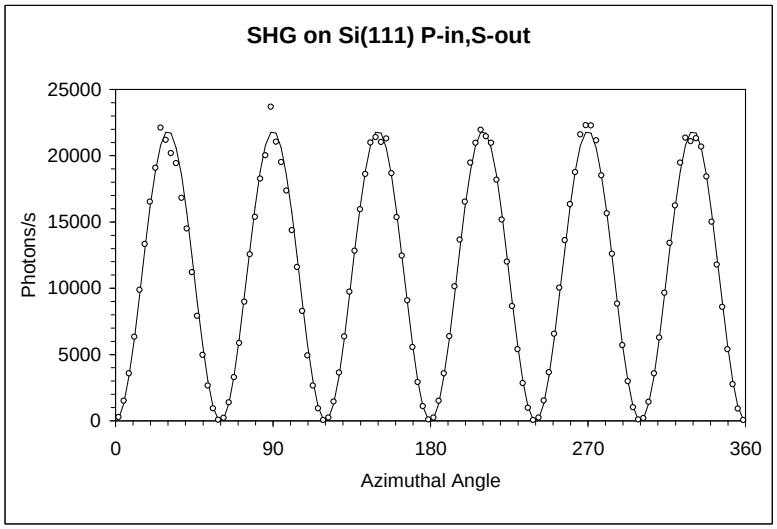

Figure 4.22: *SHG from Si(111) in P-in, S-out configuration at input power of 40mW*

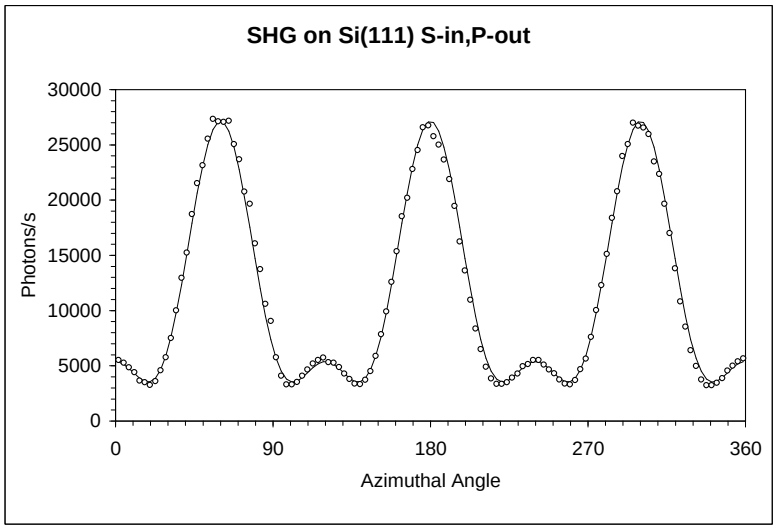

Figure 4.23: *SHG from Si(111) in S-in, P-out configuration at input power of 40mW*

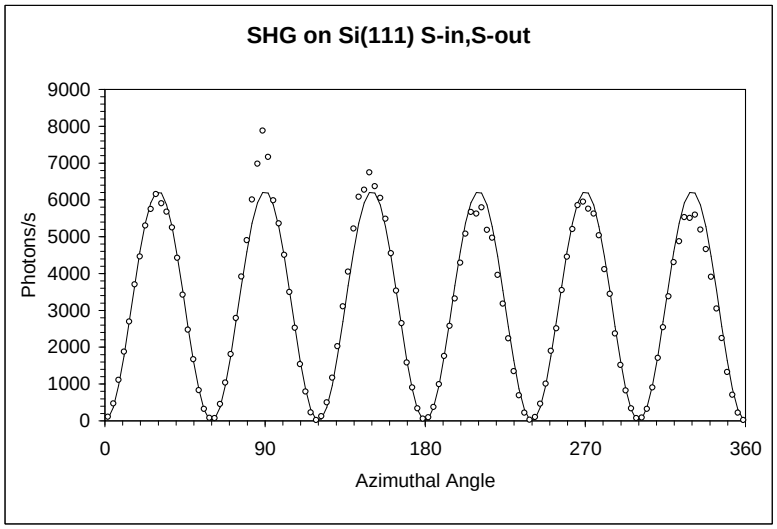

Figure 4.24: *SHG from Si(111) in S-in, S-out configuration at input power of 40mW*

4.6.2 Third Harmonic Signal

The THG signal from Si(111) presented in Figs. [4.25] thru [4.28] is well described by the dipole bulk polarization (see Table 3.5). The P-in, P-out signal is relatively smooth but the data can be fitted over a wide range of the fit parameters b_{pp} and α, when they are changed simultaneously. Like for Si(110) it is extremely hard to isolate the P-in, S-out and P-in,S-out configurations, as the signal levels of P-in, P-out and S-in, S-out are even 600 and 6000 times higher, respectively. While the six peaks of the S-in, P-out signal changed only their heights near the optimal position of the polarizers, the signal from the S-in, P-out configuration did not show the expected six equally high peaks. The only information from the SP polarization configuration is that the signal is very weak.

The used fit functions are:

P-in, P-out: $|a_{pp}e^{i\alpha} + b_{pp}\cos(3\phi)^2|^2$

$a_{pp} = 305 \pm 3, b_{pp} = 25 \pm 12, \alpha = 41^\circ \pm 20^\circ$

P-in, S-out: $|b_{ps}\sin(3\phi)|^2$

$b_{ps} = 13.7 \pm 0.5$

S-in, P-out: $|b_{sp}\sin(3\phi)|^2$

$b_{ps} = 4.1 \pm 4$ (bad fit)

S-in, S-out: $|a_{ss}|^2$

$a_{pp} = 152 \pm 24$

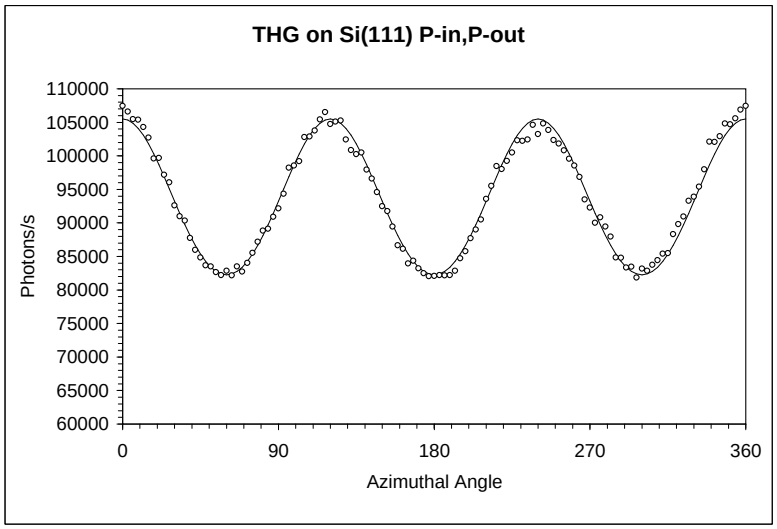

Figure 4.25: *THG from Si(111) in P-in, P-out configuration at input power of 6mW*

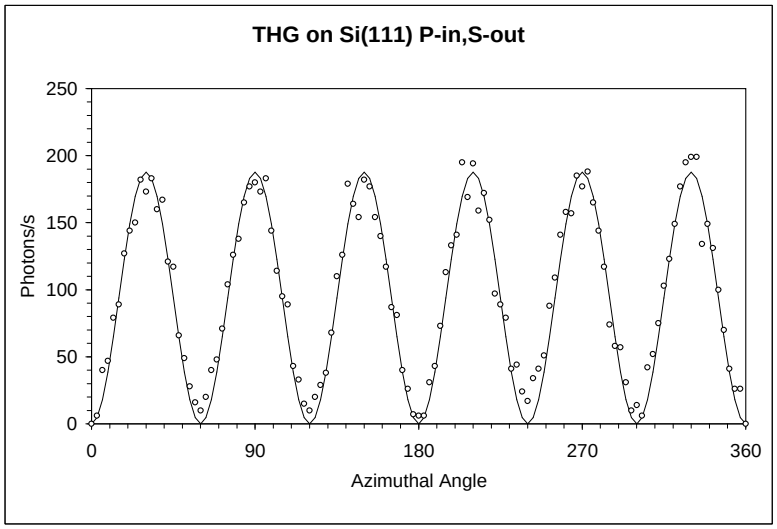

Figure 4.26: *THG from Si(111) in P-in, S-out configuration at input power of 6mW*

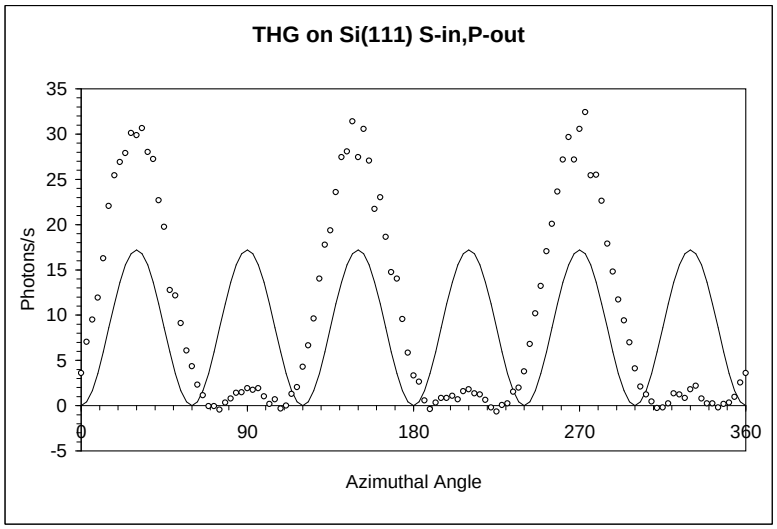

Figure 4.27: *THG from Si(111) in S-in, P-out configuration at input power of 6mW*

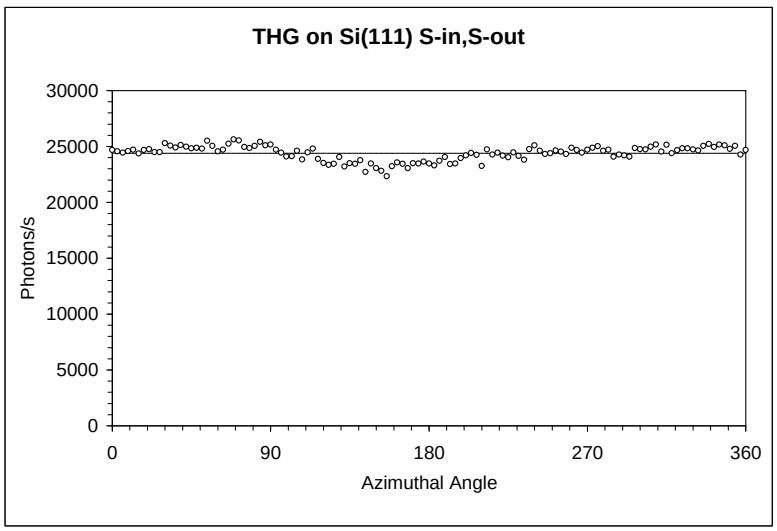

Figure 4.28: *THG from Si(111) in S-in, S-out configuration at input power of 6mW*

4.6.3 Fourth Harmonic Signal

The fit functions the FHG signal from Si(111) shown in Figs. [4.29] thru [4.32] have to include bulk quadrupole terms with their unique six-fold azimuthal contribution in order to model the unequal distance between the peaks in the P-in, S-out and S-in, S-out configuration. In figures show also the best fits under the constrain of no six-fold polarization contribution. These curves cannot model the slightly broadened peaks in P-in, P-out and S-in, P-out and the unequal spacing of the peaks in P-in, S-out and S-in, S-out configuration. For a realistic fit of the P-in, S-out and S-in, S-out data an offset was taken into account as well. Since the offset is much higher than the background noise of about 1 count per 10s another source must be present. One possibility would be surface roughness which was also mentioned in the FHG measurement for Si(110).

The used fit functions are:

P-in, P-out: $|a_{pp}e^{i\alpha} + b_{pp}e^{i\beta}\cos(3\phi) + c_{pp}\cos(6\phi)|^2$

where $a_{pp}e^{i\alpha} = a^S_{pp} + a^Q_{pp}$, $b_{pp} = b^S_{pp} + b^Q_{pp}$

$a_{pp} = 24.0 \pm 1.0, b_{pp} = 13.8 \pm 1.0, c_{pp} = 9.4 \pm 3.0, \alpha = 250° \pm 60°, \beta = 58° \pm 60°$

P-in, S-out: $o_{ps} + |b_{ps}e^{i\beta}\sin(3\phi) + c_{ps}\sin(6\phi)|^2$

where $a_{pp}e^{i\alpha} = a^S_{pp} + a^Q_{pp}$, $b_{pp} = b^S_{pp} + b^Q_{pp}$

$o_{ps} = 5.6 \pm 2.5, b_{ps} = 5.7 \pm 0.5, c_{ps} = 0.73 \pm 0.3, \beta = 0°$

S-in, P-out: $|a_{sp}e^{i\alpha} + b_{sp}e^{i\beta}\cos(3\phi) + c_{sp}\cos(6\phi)|^2$

where $a_{pp}e^{i\alpha} = a^S_{pp} + a^Q_{pp}$, $b_{pp} = b^S_{pp} + b^Q_{pp}$

$a_{sp} = 3.12 \pm 0.12, b_{sp} = 3.54, c_{sp} = 0.78 \pm 0.3, \alpha = 49° \pm 5°, \beta = 146° \pm 15°$

S-in, S-out: $o_{ss} + |b_{ss}e^{i\beta}\sin(3\phi) + c_{ss}\sin(6\phi)|^2$

where $a_{pp}e^{i\alpha} = a_{pp}^S + a_{pp}^Q$, $b_{pp} = b_{pp}^S + b_{pp}^Q$

$o_{ss} = 20.4 \pm 3.0, b_{ss} = 4.36 \pm 0.20, c_{ss} = 0.64 \pm 0.32, \beta = 135° \pm 15°$

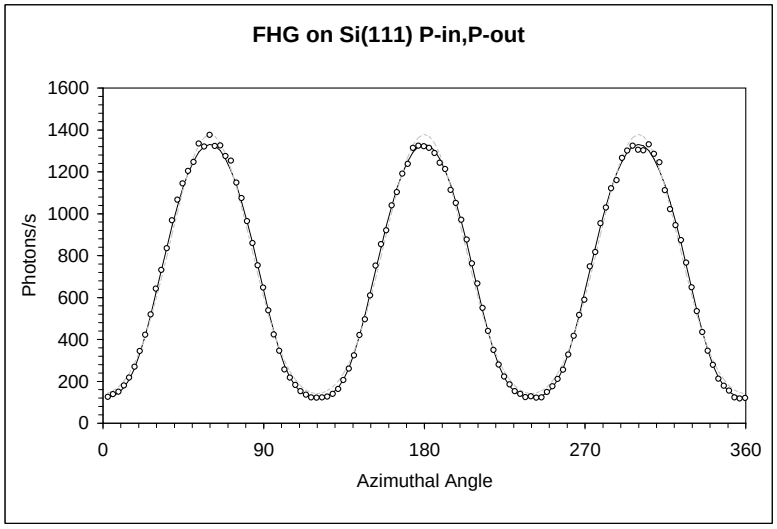

Figure 4.29: *FHG from Si(111) in P-in, P-out configuration at input power of 350mW*

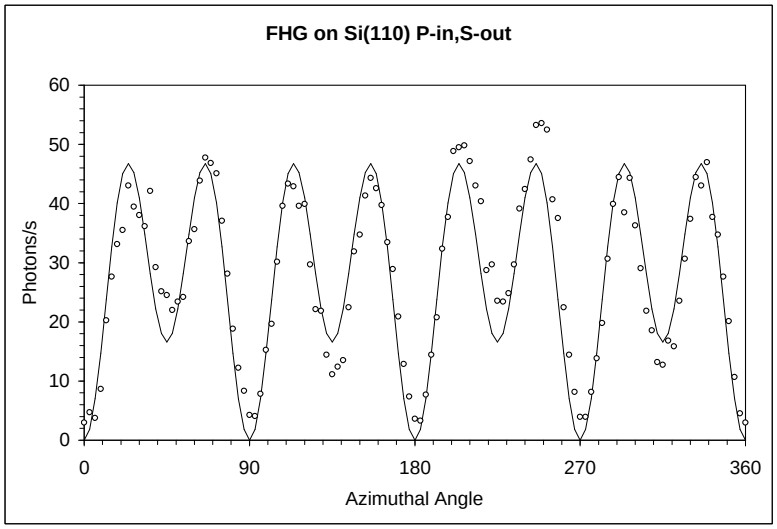

Figure 4.30: *FHG from Si(111) in P-in, S-out configuration at input power of 350mW*

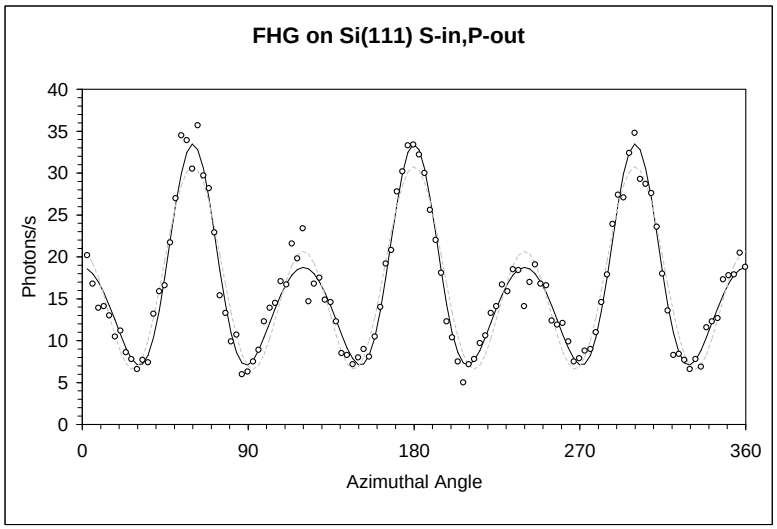

Figure 4.31: *FHG from Si(111) in S-in, P-out configuration at input power of 350mW*

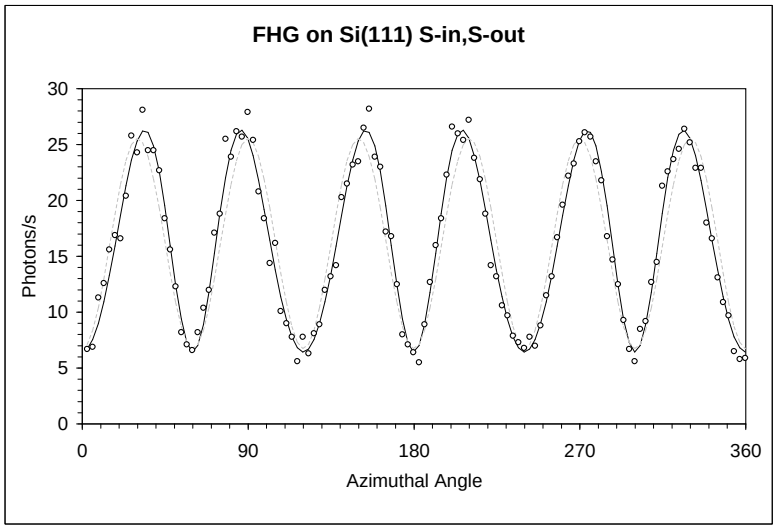

Figure 4.32: *FHG from Si(111) in S-in, S-out configuration at input power of 350mW*

Chapter 5

Conclusions

In this thesis a program was presented that enables to calculate symmetry properties of nonlinear susceptibility tensors. The problem was handled in a most general way that it is possible to do these calculations in principle for arbitrary large tensor and arbitrary symmetry transformations. With the help of this program the full analysis of the third and fourth harmonic susceptibility tensors were done for all crystal classes.

With the second part of the program the dependence on surface orientation, Fresnel factors, incident and azimuthal angle and the non-zero elements of the applying dipole and quadrupole tensors of SHG, THG and FHG from Si(110), GaAs(011), Si(111) and GaAs(011) were derived. A calculation for reconstructed GaAs(100) surfaces showed a possible change of the SHG signal when the reconstruction changes from a Ga to As rich surface.

Using an amplified, pulsed 200 fs laser the azimuthal dependence of second, third and fourth harmonic signals from Si(110) and Si(111) surfaces were measured. The signals fit well with the derived formulas for the macroscopic picture of the nonlinear polarization. In these surface orientations the bulk quadrupole contribution to the signal can only be separated if its higher rank can resolve a higher rotational

symmetry. In all of these cases- SHG and FHG from Si(110) and FHG from Si(111)- an indication for a contribution of the bulk quadrupole tensor was found. It shows that the quadrupole contribution to the fourth harmonic signal can be detected.

Appendix A

Program for Dipole Tensors

This chapter contains the code of the program that was written to study the symmetry properties of susceptibility tensors. Comments are printed in boxes framed by '>'.

```
>>>>>>>>>>>>>>>>>>>>>>>>>>>>>>>>>>>>>>>>>>>>>>>>>>>>>>>>>>>>>>>>>>>>>>>>>>>>>>>>>>>>>>>>>>>>>>>>>>>>>>>
> Nonzero Tensor Elements of \!\(TraditionalForm\`X\^\((2, 3, 4)\)\)                                    >
> This program allows to calculate the nonzero components of nonlinear quadrupole tensors X and their   >
> relationship. With "Initialization" one has to select the rank of the tensor, the symmetry operations, >
> which leaves the crystal invariant and choose, if the calculation should also use the intrinsic       >
> permutation symmetry of the last n-2 indices that is given by n-th harmonic generation.               >
> Please be patient, as the computer does it's calculations after the input.                            >
> This section must be evaluated before using the later sections.                                       >
> To calculate the angular dependence the program has to know the (hkl)-direction that is perpendicular >
> to the surface. Then SS, SP, PS and PP configurations are calculated. The output is normalized with E^(n-1).  >
>                                                                                                       >
> Initialization (start me first)                                                                       >
>                                                                                                       >
> To include further symmetries, add '{"description",{matrix1,matrix2,..}},' within the brackets of 'operations'>
>>>>>>>>>>>>>>>>>>>>>>>>>>>>>>>>>>>>>>>>>>>>>>>>>>>>>>>>>>>>>>>>>>>>>>>>>>>>>>>>>>>>>>>>>>>>>>>>>>>>>>

Clear["Global`*"]
Off[General::spell1]
Needs["LinearAlgebra`MatrixManipulation`"]

(******* Choose dimension *******)
dim=Input["Dimension of Tensor:\nType `n` for (n-2)th harmonics.\nE.g. `6` for 4th-harmonics"];

(******* Choose symmetry operations *******)
Module[{z,str,operations,dz,
        dx2={{ 1,0,0},{0,-1,0},{0,0,-1}},        (*3 rotational symmetries*)
        dy2={{-1,0,0},{0, 1,0},{0,0,-1}},
        xyz={{0,0, 1},{ 1,0,0},{0, 1,0}},
        xy    ={{0, 1,0},{ 1,0,0},{0,0, 1}},     (*4 mirror symmetries*)
        zminusz={{ 1,0,0},{0, 1,0},{0,0,-1}},
        xminusx={{-1,0,0},{0, 1,0},{0,0, 1}},
```

```
        yminusy={{ 1,0,0},{0,-1,0},{0,0, 1}}},
{dz[n_Integer]:={{Cos[2 Pi/n],-Sin[2 Pi/n],0},{Sin[2 Pi/n],Cos[2 Pi/n],0},{0,0,1}};
 (*Schoenflies not.: axis like in Wyckhoff, The Structure Of Crystals, 1931*)
 operations={
      {"c1 ",{ IdentityMatrix}},              (* 1 *)       (*tricinic*)
      {"ci ",{-IdentityMatrix[3]}},           (* 1- *)
      {"cs ",{yminusy}},                      (* m *)       (*monoclinic*)
      {"c2 ",{dy2}},                          (* 2 *)
      {"c2h",{dy2,yminusy}},                  (* 2/m *)
      {"c2v",{dz[2],yminusy}},                (* 2mm *)     (*orthorombic*)
      {"d2 ",{dz[2],dx2}},                    (* 222,v *)
      {"d2h",{dz[2],yminusy,dx2}},            (* mmm,vh *)
      {"s4 ",{-dz[4]}},                       (* 4- *)      (*tetragonal*)
      {"d2d",{dz[2],dx2,xy}},                 (* 4-2m,vd *)
      {"c4 ",{dz[4]}},                        (* 4 *)
      {"c4h",{dz[4],zminusz}},                (* 4/m *)
      {"c4v",{dz[4],xminusx}},                (* 4mm *)
      {"d4 ",{dz[4],dx2}},                    (* 422 *)
      {"d4h",{dz[4],dx2,zminusz}},            (* 4/mmm *)
      {"t  ",{xyz,dz[2]}},                    (* 23 *)      (*cubic*)
      {"th ",{xyz,dz[2],zminusz}},            (* m3 *)
      {"td ",{xyz,dz[2],xy}},                 (* 4-3m *)
      {"o  ",{xyz,dz[4]}},                    (* 432 *)
      {"oh ",{xyz,dz[4],zminusz}},            (* m3m *)
      {"c3 ",{ dz[3]}},                       (* 3 *)       (*trigonal*)
      {"c3i",{-dz[3]}},                       (* 3- *)
      {"c3v",{ dz[3],xminusx}},               (* 3m *)   (*mirror pl perp to x*)
      {"d3 ",{ dz[3],dx2}},                   (* 32 *)
      {"c3d",{-dz[3],dx2}},                   (* 3-m,d3d *)
      {"c3h",{dz[3].zminusz}},                (* 6- *)      (*hexagonal*)
      {"d3h",{dz[3].zminusz,dx2}},            (* 6-m2 *)
      {"c6 ",{dz[6]}},                        (* 6 *)
      {"c6h",{dz[6],zminusz}},                (* 6/m *)
      {"c6v",{dz[6],yminusy}},                (* 6mm *)
      {"d6 ",{dz[6],dx2}},                    (* 622 *)
      {"d6h",{dz[6],dx2,zminusz}},            (* 6/mmm *)
      {"isotropic",{dz[17],xminusx}}
};
 str="Choose symmetries:\n| ";
 For[z=1,z<=Length[operations],z=z+1,
     str=str <> ToString[z] <> " : " <> operations[[z]][[1]] <> " | "];
 symm=operations[[Input[str]]][[2]]//N;   (*Symmetry matrices for specific problem*)
}];

(******* intrinsic symmetry y/n *******)
createvector:=
Module[{x={},
        v=Table[3^(dim-i),{i,2,dim}],
        b={""},
        m,nulllist,newlist},
{Do[b=Flatten[Table[{"0","1","2"}[[i]]<>b[[j]],{i,3},{j,Length[b]}]],{dim-1}];
 Do[b[[i]]=ToExpression[Sort[Characters[b[[i]]]]].v,{i,1,Length[b]}];
 m=Max[b]+1;
 b=m-b;
 nulllist=Table[0,{i,3^(dim-1)}];
```

```
 While[m>0,
 {newlist=ReplacePart[nulllist,1,Position[b,m]];
  b=b-m*newlist;
  x=AppendTo[x,newlist];
  m=Max[b]}];
 BlockMatrix[Outer[Times,IdentityMatrix[3],x]]
}][[1]]


If[Input["To include intrinsic symmetry for n-th harmonics, type '1'."]==1,
   {x=Transpose[createvector];},
   x=IdentityMatrix[3^dim];];


(******* Subroutines for main program *******)

vectortomatrix[vec_]:=If[VectorQ[vec],{vec},vec]

lines[m_List]:=Dimensions[m][[1]]

rows[m_List] :=Dimensions[m][[2]]

eulerbackward[mat_List]:=
Module[{len=lines[mat],m=mat,pos},
{While[len>0,
 {pos=Flatten[Position[Sign[Abs[m[[len]]]],1]][[1]];
  If[pos>0,
     {m[[len]]=Chop[m[[len]]/m[[len,pos]]],
      Do[m[[i]]=Chop[m[[i]]-m[[i,pos]]*m[[len]]],{i,1,len-1}]}],
  len=len-1}];
 m=vectortomatrix[m]}][[1]]


pickcolumn[mat_List,vec_List]:=
Block[{m2={}},
{Do[m2=Join[m2,{Transpose[mat][[vec[[i]]]]}],{i,Length[vec]}];
 m2=vectortomatrix[m2];
 m2=Transpose[m2]}][[1]]


findcolumn[mat_List]:=
Module[{m,j=1,liste={}},
{m=Join[mat,{Table[0,{za,rows[mat]}]}];
 Do[If[m[[j,i]]==0,
       liste=Join[liste,{i}],
       j=j+1],
    {i,rows[mat]}];
 liste}][[1]]


sortrow[mat_List,col_Integer]:=
Block[{m,v,p},
{m=vectortomatrix[mat];
 v=Abs[Transpose[m][[col]]];
 p=Flatten[Position[v,Max[v]]][[1]];
```

```
 v=m[[1]];
 m[[1]]=m[[p]];
 m[[p]]=v;
 m}][[1]]


eulerforward[mat_List]:=
Block[{m,pos,mrows=rows[mat],b={}},
{m=Chop[Table[mat[[i]]/Max[Abs[mat[[i]]],1],{i,Length[mat]}]];
 m=Join[m,{Table[0,{i,mrows}]}];
 pos=1;
 While[pos<=mrows,
       {m=sortrow[m,pos];
        If[m[[1,pos]]!=0,
           {m[[1]]=Chop[m[[1]]/m[[1,pos]]],
            Do[m[[i]]=Chop[m[[i]]-m[[i,pos]]*m[[1]]],{i,2,Length[m]}],
            AppendTo[b,m[[1]]],
            m=Delete[m,1]}];
         pos=pos+1}];
 vectortomatrix[b]}][[1]]


findnullspace[mat_]:=
Block[{m,m2,lst,len,zauber},
{m=vectortomatrix[mat];
 If[Max[Chop[Abs[m]]]==0,
    m2=IdentityMatrix[rows[m]],
    {len=rows[m];
     m=eulerforward[m];
     m=eulerbackward[m];
     lst=findcolumn[m];
     If[lst=={},
        m2=Table[{0},{i,len}],
        {
         m=pickcolumn[m,lst];
         zauber=Complement[Table[i,{i,len}],lst];
         m2=Table[0,{j,len},{i,Max[Length[lst],1]}];
         Do[Do[m2[[zauber[[j]],i]]=-m[[j,i]],{i,rows[m]}],{j,lines[m]}];
         Do[m2[[lst[[i]],i]]=1,{i,Length[lst]}];
        }
       ];
    };
 ];
 m2}][[1]]



(****** Main program: determination of relationship between tensor elements *****)
For[z=1,z<=Length[symm],z=z+1,
    {mt=Transpose[symm[[z]]],

     m =Inverse[symm[[z]]],
     Do[m=BlockMatrix[Outer[Times,m,mt]],{dim-1}],
     m=m.x-x,
     inv=findnullspace[m];
```

```
     x=Chop[x.inv]}]

x=Rationalize[x,10^(-10)];
x=Transpose[x];
If[Max[x]!=0,{x=eulerforward[x],x=eulerbackward[x]}];

chi=Transpose[x].Table["X"<>ToString[i],{i,Length[x]}];
Do[chi=Partition[chi,3],{dim}]
Nonzero elements and their relationship
(run Initialization first)
readout={""};
Do[readout=Flatten[Table[{"x","y","z"}[[i]]<>readout[[j]],{i,3},
                         {j,Length[readout]}]],{dim}]


>>>>>>>>>>>>>>>>>>>>>>>>
> (*Non zero elements*) >
>>>>>>>>>>>>>>>>>>>>>>>>
   y=Apply[Plus,Sign[Abs[x]]];
   output1=readout[[Flatten[Position[Sign[y],1]]]];
   Print[Length[Position[Sign[y],1]]," non-zero tensor elements: (dependend on ",
         Length[x]," parameters)"]
   Print[output1]
   Print[""]

(*Relationship between non-zero elements*)
   output2=" ";
   If[Apply[Plus,Chop[y^2-y]]!=0,
      {Print["Tensor elements are not separable."],
       Print["'readout' = Flatten[chi]"]},
      {Do[{maximum=Max[x[[i]]],
           Do[If[x[[i,j]]!=0,
                 output2=output2<>ToString[readout[[j]]*maximum/x[[i,j]]]<>" = "],
              {j,3^dim}],
            output2=output2 <> ToString[maximum*X] <> ToString[i]<>" \n "},
           {i,Length[x]}],
       Print[Length[x]"Independent tensor elements:"],
       Print[output2]}];


>>>>>>>>>>>>>>>>>>>>>>>>>>>>>>>>>>>>>>>>>>>>>>>>>>>>>>>>>>>>>>>>>>>>>>>>>>>>>>>
> Angular dependence of the signal in reflection (run Initialization first) >
>>>>>>>>>>>>>>>>>>>>>>>>>>>>>>>>>>>>>>>>>>>>>>>>>>>>>>>>>>>>>>>>>>>>>>>>>>>>>>>

a=IdentityMatrix[3];

a[[1,3]]=Input["Insert (h)"];
a[[2,3]]=Input["Insert (k)"];
a[[3,3]]=Input["Insert (l)"];
a=a/Sqrt[a[[1,3]]^2+a[[2,3]]^2+a[[3,3]]^2];

If[N[a[[2,3]]]==0.,
   a[[2,2]]=1,
   a[[2,2]]=Sqrt[ a[[3,3]]^2 / (a[[3,3]]^2+a[[2,3]]^2)]];
```

```
If[N[a[[3,3]]]==0.,
   a[[3,2]]=-Sign[a[[2,3]]],
   a[[3,2]]=-Sign[a[[2,3]] a[[3,3]]] Sqrt[1-a[[2,2]]^2]];

a[[1,1]]= a[[2,2]] a[[3,3]]-a[[3,2]] a[[2,3]];
a[[2,1]]= a[[3,2]] a[[1,3]];
a[[3,1]]=-a[[2,2]] a[[1,3]];
a=Chop[a];

picture=Show[Graphics3D[{Polygon[{{-0.3,-0.3,0},{-0.3,0.3,0},{0.3,0.3,0},{0.3,-0.3,0}}],
                         Line[{{0,0,0},a[[1]]}],Text["x",0.9 a[[1]]],
                         Line[{{0,0,0},a[[2]]}],Text["y",0.9 a[[2]]],
                         Line[{{0,0,0},a[[3]]}],Text["z",0.9 a[[3]]],

                         Line[{{0,0,0},{1,0,0}}],Text["e1",{1.1,0,0}],
                         Line[{{0,0,0},{0,1,0}}],Text["e2",{0,1.1,0}],
                         Line[{{0,0,0},{0,0,1}}],Text["e3",{0,0,1.1}]},
                        Boxed->False]];

(* delete linear Fresnel factors *)
Clear[lfx,lfy,lfz];

Print["Angular dependence of signal:"]

Print["\nSS configuration:"]
ss=chi;
Do[ss =ss.(a.{-Sin[\[Alpha]] lfy,Cos[\[Alpha]] lfy,0}),{dim-1}];
ss=(ss.(a.{-Sin[\[Alpha]] fy,Cos[\[Alpha]] fy,0}))[[1]]//Expand//Chop//TrigReduce//Factor;
Print[ss]

Print["\nSP configuration:"]
spx=chi;
Do[spx=spx.(a.{-Sin[\[Alpha]] lfy,Cos[\[Alpha]] lfy,0}),{dim-1}];
spx=(spx.(a.{Cos[\[Alpha]] fx, Sin[\[Alpha]] fx, 0}))[[1]]//Expand//Chop//TrigReduce//Factor;
spz=chi;
Do[spz=spz.(a.{-Sin[\[Alpha]] lfy,Cos[\[Alpha]] lfy,0}),{dim-1}];
spz=(spz.(a.{0,0,fz}))[[1]]//Expand//Chop//TrigReduce//Factor;
Print[spx," +\n",spz]

Print["\nPS configuration:"]
ps=chi;
Do[ps =ps.(a.{Cos[\[Alpha]] lfx,Sin[\[Alpha]] lfx,lfz}),{dim-1}];
ps=(ps.(a.{-Sin[\[Alpha]] fy,Cos[\[Alpha]] fy,0}))[[1]]//Expand//Chop//TrigReduce//Factor;
Print[ps]

Print["\nPP configuration:"]
ppx=chi;
Do[ppx=ppx.(a.{Cos[\[Alpha]] lfx,Sin[\[Alpha]] lfx,lfz}),{dim-1}];
ppx=(ppx.(a.{Cos[\[Alpha]] fx, Sin[\[Alpha]] fx, 0}))[[1]]//Expand//Chop//TrigReduce//Factor;
ppz=chi;
Do[ppz=ppz.(a.{Cos[\[Alpha]] lfx,Sin[\[Alpha]] lfx,lfz}),{dim-1}];
ppz=(ppz.(a.{0,0,fz}))[[1]]//Expand//Chop//TrigReduce//Factor;
Print[ppx," +\n",ppz]
```

```
>>>>>>>>>>>>>>>>>>>>>>>>>>>>>>>>>>>>>>>>>>>>>>>>>>>>>>>>>>>>>>>>>>>>>>>>
> Graphs (run Initialization and Angular dependence first) >
>>>>>>>>>>>>>>>>>>>>>>>>>>>>>>>>>>>>>>>>>>>>>>>>>>>>>>>>>>>>>>>>>>>>>>>>

(* refracted index of fundamental and harmonic signal *)
\[Epsilon]fundamental=3.692^2;
\[Epsilon]harmonic   =1.831^2;

(*linear Fresnel factors*)
lfy=2 Cos[\[Theta]]/(Cos[\[Theta]]+Sqrt[\[Epsilon]fundamental-Sin[\[Theta]]^2]);
lfx=2 Cos[\[Theta]] Sqrt[\[Epsilon]fundamental-Sin[\[Theta]]^2]
        /(\[Epsilon]fundamental Cos[\[Theta]]+Sqrt[\[Epsilon]fundamental-Sin[\[Theta]]^2]);
lfz=2 Cos[\[Theta]] Sin[\[Theta]]
        /(\[Epsilon]fundamental Cos[\[Theta]]+Sqrt[\[Epsilon]fundamental-Sin[\[Theta]]^2]);

(* nonlinear Fresnel factors *)
fresnels [e_,e4_,t_]=
   4 Pi/(e-e4) (Sqrt[e4-Sin[t]^2]-Sqrt[e-Sin[t]^2])/(Sqrt[e4-Sin[t]^2]+Cos[t]);
fresnelp [e_,e4_,t_]=4 Pi /(Sqrt[e-Sin[t]^2]+Sqrt[e4-Sin[t]^2])/
                    (Sqrt[e4-Sin[t]^2]+e4 Cos[t]);
fresnelpx[e_,e4_,t_]=fresnelp[e,e4,t] Sqrt[e4-Sin[t]^2];
fresnelpz[e_,e4_,t_]=fresnelp[e,e4,t] Sin[t];
fy=fresnels [\[Epsilon]fundamental,\[Epsilon]harmonic,\[Theta]];
fx=fresnelpx[\[Epsilon]fundamental,\[Epsilon]harmonic,\[Theta]];
fz=fresnelpz[\[Epsilon]fundamental,\[Epsilon]harmonic,\[Theta]];
(* various plots *)
Plot[ss^2       /.{\[Theta]->Pi/4.0,"X1"->5,"X2"->1},{\[Alpha],0,2 Pi}];
Plot[(spx+spz)^2/.{\[Theta]->Pi/4.0,"X1"->5,"X2"->1},{\[Alpha],0,2 Pi}];
Plot[ps^2       /.{\[Theta]->Pi/4.0,"X1"->5,"X2"->1},{\[Alpha],0,2 Pi}];
Plot[(ppx+ppz)^2/.{\[Theta]->Pi/4.0,"X1"->5,"X2"->1},{\[Alpha],0,2 Pi}];
Plot3D[ss^2/.{"X1"->5,"X2"->1}
       ,{\[Alpha],0,2 Pi},{\[Theta],0,Pi/2},PlotPoints->50];
Plot3D[(spx+spz)^2/.{"X1"->5,"X2"->1}
       ,{\[Alpha],0,2 Pi},{\[Theta],0,Pi/2},PlotPoints->50];
Plot3D[ps^2/.{"X1"->5,"X2"->1}
      ,{\[Alpha],0,2 Pi},{\[Theta],0,Pi/2},PlotPoints->50];
Plot3D[(ppx+ppz)^2/.{"X1"->5,"X2"->1}
       ,{\[Alpha],0,2 Pi},{\[Theta],0,Pi/2},PlotPoints->50];
```

Appendix B

Modifications for Quadrupole Tensors

The symmetry analysis of quadrupole susceptibility tensors is similar to the analysis of the dipole tensors. The two main differences are that first the intrinsic permutation symmetry of a n-th rank quadrupole tensor is only valid for the last $n-2$ indices. The second difference lies in the analysis. Instead of electric field vectors a wave vector has once to be multiplied with the tensor.

Changes for part I of the program:

```
(******* intrinsic symmetry y/n *******)
createvector:=
Module[{x={},
        v=Table[3^(dim-i),{i,3,dim}],
        b={""},
        m,nulllist,newlist},
{Do[b=Flatten[Table[{"0","1","2"}[[i]]<>b[[j]],{i,3},{j,Length[b]}]],{dim-2}];
 Do[b[[i]]=ToExpression[Sort[Characters[b[[i]]]]].v,{i,1,Length[b]}];
 m=Max[b]+1;
 b=m-b;
 nulllist=Table[0,{i,3^(dim-2)}];
 While[m>0,
 {newlist=ReplacePart[nulllist,1,Position[b,m]];
  b=b-m*newlist;
  x=AppendTo[x,newlist];
  m=Max[b]}];
 BlockMatrix[Outer[Times,IdentityMatrix[3],BlockMatrix[Outer[Times,IdentityMatrix[3],x]]]]
}][[1]]
```

Changes for part III of the program:

```
Print["Angular dependence of signal:"]

Print["\nSS configuration:"]
ss=chi;
Do[ss =ss.(a.{-Sin[\[Alpha]] lfy,Cos[\[Alpha]] lfy,0}),{dim-2}];
ss= ss.(a.{Cos[\[Alpha]] kx,Sin[\[Alpha]] kx,kz});
ss=(ss.(a.{-Sin[\[Alpha]] fy,Cos[\[Alpha]] fy,0}))[[1]]//Expand//Chop//TrigReduce//Factor;
Print[ss]

Print["\nSP configuration:"]
spx=chi;
Do[spx=spx.(a.{-Sin[\[Alpha]] lfy,Cos[\[Alpha]] lfy,0}),{dim-2}];
spx= spx.(a.{Cos[\[Alpha]] kx,Sin[\[Alpha]] kx,kz});
spx=(spx.(a.{Cos[\[Alpha]] fx, Sin[\[Alpha]] fx, 0}))[[1]]//Expand//Chop//TrigReduce//Factor;
spz=chi;
Do[spz=spz.(a.{-Sin[\[Alpha]] lfy,Cos[\[Alpha]] lfy,0}),{dim-2}];
spz= spz.(a.{Cos[\[Alpha]] kx,Sin[\[Alpha]] kx,kz});
spz=(spz.(a.{0,0,fz}))[[1]]//Expand//Chop//TrigReduce//Factor;
Print[spx," +\n",spz]

Print["\nPS configuration:"]
ps=chi;
Do[ps =ps.(a.{Cos[\[Alpha]] lfx,Sin[\[Alpha]] lfx,lfz}),{dim-2}];
ps= ps.(a.{Cos[\[Alpha]] kx,Sin[\[Alpha]] kx,kz});
ps=(ps.(a.{-Sin[\[Alpha]] fy,Cos[\[Alpha]] fy,0}))[[1]]//Expand//Chop//TrigReduce//Factor;
Print[ps]

Print["\nPP configuration:"]
ppx=chi;
Do[ppx=ppx.(a.{Cos[\[Alpha]] lfx,Sin[\[Alpha]] lfx,lfz}),{dim-2}];
ppx= ppx.(a.{Cos[\[Alpha]] kx,Sin[\[Alpha]] kx,kz});
ppx=(ppx.(a.{Cos[\[Alpha]] fx, Sin[\[Alpha]] fx, 0}))[[1]]//Expand//Chop//TrigReduce//Factor;
ppz=chi;
Do[ppz=ppz.(a.{Cos[\[Alpha]] lfx,Sin[\[Alpha]] lfx,lfz}),{dim-2}];
ppz= ppz.(a.{Cos[\[Alpha]] kx,Sin[\[Alpha]] kx,kz});
ppz=(ppz.(a.{0,0,fz}))[[1]]//Expand//Chop//TrigReduce//Factor;
Print[ppx," +\n",ppz]
```

Appendix C

Angular Dependence of Higher Harmonic Signals for GaAs(110) and GaAs(111)

This section shows the expected contribution of the bulk dipole contribution of a crystal with $3\bar{4}m$ symmetry to the generation of second, third and fourth harmonic signals. The tensor is described in a coordinate system (x,y,z) that corresponds to the crystallographic axis [100], [010] and [001]. The convention for the Fresnel factors can be found in section 3.3.

The tensors and the azimuthal dependence of THG from GaAs(011) and GaAs(110) are qualitatively the same as for silicon. The tables can be found in section 3.3.1 and 3.3.2.

In the following tables the expected amplitudes of the electric field of the remitted light are split into an isotropic and an anisotropic part in respect to the rotation angle ϕ. The coefficients are given below.

Table C.1: *SHG bulk dipole contributions of GaAs(110)*

	Isotropic	Anisotropic (ϕ)	Anisotropic (3ϕ)
S-in, S-out	0	$b_{SS}\cos\phi$	$c_{SS}\cos 3\phi$
S-in, P-out	0	$b_{SP}\sin\phi$	$c_{SP}\sin 3\phi$
P-in, S-out	0	$b_{PS}\cos\phi$	$c_{PS}\cos 3\phi$
P-in, P-out	0	$b_{PP}\sin\phi$	$c_{PP}\sin 3\phi$

$$
\begin{aligned}
b_{SS} &= \frac{3}{4} f_y^{(2)} \chi_{xyz} f_y^2 \\
c_{SS} &= -\frac{3}{4} f_y^{(2)} \chi_{xyz} f_y^2 \\
b_{SP} &= \frac{1}{4} f_x^{(2)} \chi_{xyz} f_y^2 \\
c_{SP} &= -\frac{3}{4} f_x^{(2)} \chi_{xyz} f_y^2 \\
b_{PS} &= \frac{1}{4} f_y^{(2)} \chi_{xyz} (f_x^2 - 4 f_z^2) \\
c_{PS} &= \frac{3}{4} f_y^{(2)} \chi_{xyz} f_x^2 \\
b_{PP} &= \frac{1}{4} f_x^{(2)} \chi_{xyz} (3 f_x^2 - 4 f_z^2) - 2 f_z^{(2)} \chi_{xyz} f_x f_z \\
c_{PP} &= \frac{3}{4} f_x^{(2)} \chi_{xyz} f_x^2
\end{aligned}
$$

With one non-zero element (corresponding to $3\bar{4}m$ symmetry):

$\chi_{xyz} = \chi_{yxz} = \chi_{zxy}$

Table C.2: *SHG bulk dipole contributions of GaAs(111)*

	Isotropic	Anisotropic (3ϕ)
S-in, S-out	0	$b_{SS}\sin 3\phi$
S-in, P-out	a_{SP}	$b_{SP}\cos 3\phi$
P-in, S-out	0	$b_{PS}\sin 3\phi$
P-in, P-out	a_{PP}	$b_{PP}\cos 3\phi$

$$
\begin{aligned}
b_{SS} &= \frac{\sqrt{2}}{\sqrt{3}} f_y^{(2)} \chi_{xyz} f_y^2 \\
a_{SP} &= -\frac{1}{\sqrt{3}} f_z^{(2)} \chi_{xyz} f_y^2 \\
b_{SP} &= -\frac{\sqrt{2}}{\sqrt{3}} f_x^{(2)} \chi_{xyz} f_y^2 \\
b_{PS} &= -\frac{\sqrt{2}}{\sqrt{3}} f_y^{(2)} \chi_{xyz} f_x^2 \\
a_{PP} &= -\frac{2}{\sqrt{3}} f_x^{(2)} \chi_{xyz} f_x f_z + \\
&\quad + \frac{1}{\sqrt{3}} f_z^{(2)} \chi_{xyz} (-f_x^2 + 2 f_z^2) \\
b_{PP} &= \frac{\sqrt{2}}{\sqrt{3}} f_x^{(2)} \chi_{xyz} f_x^2
\end{aligned}
$$

With one non-zero element (corresponding to $3\bar{4}m$ symmetry):

$\chi_{xyz} = \chi_{yxz} = \chi_{zxy}$

Table C.3: *FHG bulk dipole contributions of GaAs(110)*

	Isotropic	Anisotropic(ϕ)	(3ϕ)
S-in, S-out	0	$b_{SS}\cos\phi$	$c_{SS}\cos 3\phi$
S-in, P-out	0	$b_{SP}\sin\phi$	$c_{SP}\sin 3\phi$
P-in, S-out	0	$b_{PS}\cos\phi$	$c_{PS}\cos 3\phi$
P-in, P-out	0	$b_{PP}\sin\phi$	$c_{PP}\sin 3\phi$

$$
\begin{aligned}
b_{SS} &= \frac{1}{2}f_y^{(4)}(3\chi_{xxxyz}+2\chi_{xyyyz})f_y^4 \\
c_{SS} &= -\frac{1}{2}f_y^{(4)}(3\chi_{xxxyz}+2\chi_{xyyyz})f_y^4 \\
b_{SP} &= \frac{1}{2}f_x^{(4)}\chi_{xyyyz}f_y^4 \\
c_{SP} &= -\frac{3}{2}f_x^{(4)}\chi_{xyyyz}f_y^4 \\
b_{PS} &= \frac{1}{2}f_y^{(4)}\chi_{xyyyz}(f_x^2-4f_z^2)(f_x^2+f_z^2) \\
c_{PS} &= \frac{3}{2}f_y^{(4)}\chi_{xyyyz}f_x^2(f_x^2+f_z^2) \\
b_{PP} &= \frac{1}{2}f_x^{(4)}((3\chi_{xxxyz}+2\chi_{xyyyz})f_x^4-3(4\chi_{xxxyz}-\chi_{xyyyz})f_z^2f_x^2-4\chi_{xyyyz}f_z^4)+ \\
&\quad +\frac{1}{2}f_z^{(4)}(3(\chi_{xxxyz}-3\chi_{xyyyz})f_x^2-4(3\chi_{xxxyz}+\chi_{xyyyz})f_z^2)f_xf_z \\
c_{PP} &= \frac{1}{2}f_x^{(4)}((3\chi_{xxxyz}+2\chi_{xyyyz})f_x^2+3\chi_{xyyyz}f_z^2)f_x^2+ \\
&\quad +\frac{1}{2}f_z^{(4)}(3\chi_{xxxyz}-\chi_{xyyyz})f_x^3f_z
\end{aligned}
$$

With two non-zero element (corresponding to $3\bar{4}m$ symmetry):

$\chi_{xxxyz}=\chi_{yxyyz}=\chi_{zxyzz}$,

$\chi_{xyyyz}=\chi_{xyzzz}=\chi_{yxxxz}=\chi_{yxzzz}=\chi_{zxxxy}=\chi_{zxyyy}$

Table C.4: *FHG bulk dipole contributions of GaAs(111)*

	Isotropic	Anisotropic (3ϕ)
S-in, S-out	0	$b_{SS}\sin 3\phi$
S-in, P-out	a_{SP}	$b_{SP}\cos 3\phi$
P-in, S-out	0	$b_{PS}\sin 3\phi$
P-in, P-out	a_{PP}	$b_{PP}\cos 3\phi$

$$
\begin{aligned}
b_{SS} &= \frac{2\sqrt{2}}{3\sqrt{3}} f_y^{(4)} (3\chi_{xxxyz} + 2\chi_{xyyyz}) f_y^4 \\
a_{SP} &= -\frac{2}{\sqrt{3}} f_z^{(4)} \chi_{xyyyz} f_y^4 \\
b_{SP} &= -\frac{2\sqrt{2}}{\sqrt{3}} f_x^{(4)} \chi_{xyyyz} f_y^4 \\
b_{PS} &= -\frac{2\sqrt{2}}{\sqrt{3}} f_y^{(4)} \chi_{xyyyz} f_x^2 (f_x^2 + f_z^2) \\
a_{PP} &= \frac{2}{3\sqrt{3}} f_x^{(4)} (-3(3\chi_{xxxyz} + \chi_{xyyyz}) f_x^2 + (6\chi_{xxxyz} - 8\chi_{xyyyz}) f_z^2) f_x f_z + \\
&\quad + \frac{2}{3\sqrt{3}} f_z^{(4)} (-3\chi_{xyyyz} f_x^4 - 3(3\chi_{xxxyz} - 2\chi_{xyyyz}) f_x^2 f_z^2 + (6\chi_{xxxyz} + 4\chi_{xyyyz}) f_z^4) \\
b_{PP} &= \frac{2\sqrt{2}}{3\sqrt{3}} f_x^{(4)} ((3\chi_{xxxyz} + 2\chi_{xyyyz}) f_x^2 + 3\chi_{xyyyz} f_z^2) f_x^2 + \\
&\quad + \frac{2\sqrt{2}}{3\sqrt{3}} f_z^{(4)} (3\chi_{xxxyz} - \chi_{xyyyz}) f_x^3 f_z
\end{aligned}
$$

With two non-zero element (corresponding to $3\bar{4}m$ symmetry):

$\chi_{xxxyz} = \chi_{yxyyz} = \chi_{zxyzz}$,

$\chi_{xyyyz} = \chi_{xyzzz} = \chi_{yxxxz} = \chi_{yxzzz} = \chi_{zxxxy} = \chi_{zxyyy}$

Appendix D

Symmetry Analysis for SHG for Reconstructed GaAs (100)

The most common reconstructions on GaAs surfaces dimeres form along the [110] for Ga rich surfaces and along $[\bar{1}10]$ for As rich surfaces [6]. All of these reconstructions exhibit the same surface symmetry: $2mm$. If the surface signal is strong, SHG may provide a tool to monitor the coverage of the surface by Ga and As, respectively, during the growth.

The following tables show symmetry analysis of the surface and bulk dipole contributions to the SHG signal. in both cases the coordinate system (x,y,z) has its axis along [100], [010] and [001].

The angular dependence of the SHG surface dipole polarization:

	Isotropic	Anisotropic (2ϕ)
S-in, S-out	0	0
S-in, P-out	a^S_{SP}	$b^S_{SP}\sin 2\phi$
P-in, S-out	0	$b^S_{PS}\cos 2\phi$
P-in, P-out	a^S_{PP}	$b^S_{PP}\sin 2\phi$

$$
\begin{aligned}
a^S_{SP} &= f^{(2)}_z \chi^S_{zxx} f^2_y \\
b^S_{SP} &= -f^{(2)}_z \chi^S_{zxy} f^2_y \\
b^S_{PS} &= 2 f^{(2)}_y \chi^S_{xyz} f_x f_z \\
a^S_{PP} &= 2 f^{(2)}_x \chi^S_{xxz} f_x f_z + f^{(2)}_z (\chi^S_{zxx} f^2_x + \chi^S_{zzz} f^2_z) \\
b^S_{PP} &= 2 f^{(2)}_x \chi^S_{xyz} f_x f_z + f^{(2)}_z \chi^S_{zxy} f^2_x
\end{aligned}
$$

With 5 independent tensor elements:

$\chi^S_{xxz} = \chi^S_{yyz}; \chi^S_{xyz} = \chi^S_{yxz}; \chi^S_{zxx} = \chi^S_{zyy}; \chi^S_{zxy}; \chi^S_{zzz}$

The angular dependence of the SHG bulk dipole polarization::

	Isotropic	Anisotropic
S-in, S-out	0	0
S-in, P-out	0	$b_{SP}\sin 2\phi$
P-in, S-out	0	$b_{PS}\cos 2\phi$
P-in, P-out	0	$b_{PP}\sin 2\phi$

$$
\begin{aligned}
b_{SP} &= -f_z^{(2)}\chi_{xyz}f_y^2 \\
b_{PS} &= 2f_y^{(2)}\chi_{xyz}f_x f_z \\
b_{PP} &= (2f_x^{(2)}f_x f_z + f_z^{(2)}f_x^2)\chi_{xyz}
\end{aligned}
$$

With one tensor element:

$\chi_{xyz} = \chi_{yxz} = \chi_{zxy}$

Appendix E

Coefficients for Quadrupole Contribution of FHG from Si(110) and Si(111)

The coefficients of the quadrupole tensor are described in a coordinate system (x, y, z) that corresponds to the crystallographic directions [100], [010] and [001]. The Fresnel factors are defined in section 3.3

The seven independent tensor elements are (corresponding to m3m symmetry):

$X_1 = \chi_{xxxxxx} = \chi_{yyyyyy} = \chi_{zzzzzz}$

$X_2 = \chi_{xxxxyy} = \chi_{xxxxzz} = \chi_{yyxxyy} = \chi_{yyyyzz} = \chi_{zzzzxx} = \chi_{zzzzyy}$

$X_3 = \chi_{xxyyyy} = \chi_{xxzzzz} = \chi_{yyxxxx} = \chi_{yyzzzz} = \chi_{zzxxxx} = \chi_{zzyyyy}$

$X_4 = \chi_{xxyyzz} = \chi_{yyxxzz} = \chi_{zzxxyy}$

$X_5 = \chi_{xyxxxy} = \chi_{xzxxxz} = \chi_{yxxyyy} = \chi_{yzyyyz} = \chi_{zxxzzz} = \chi_{zyyzzz}$

$X_6 = \chi_{xyxyyy} = \chi_{xzxzzz} = \chi_{yxxxxy} = \chi_{yzyzzz} = \chi_{zxxxxz} = \chi_{zyyyyz}$

$X_7 = \chi_{xyxyzz} = \chi_{xzxyyz} = \chi_{yxxyzz} = \chi_{yzxxyz} = \chi_{zxxyyz} = \chi_{zyxxyz}$

The coefficients for Si(110) quadrupole contribution are given by:

$b^Q_{SS} = \frac{1}{128}(15X_1 + 6X_2 - 15X_3 - 6X_4 - 60X_5 + 4X_6 - 24X_7) f_y^{(4)} k_x f_y^4$

$c^Q_{SS} = \frac{1}{128}(-20X_1 + 24X_2 - 20X_3 - 24X_4 - 80X_5 + 16X_6 - 96X_7) f_y^{(4)} k_x f_y^4$

d^Q_{SS}= $\frac{1}{128}(3X_1 - 18X_2 - 3X_3 + 18X_4 - 12X_5 - 12X_6 + 72X_7)f^{(4)}_y k_x f^4_y$

a^Q_{SP}=

$\frac{1}{128}(10X_1 + 84X_2 + 62X_3 + 84X_4 - 40X_5 - 40X_6 - 48X_7)f^{(4)}_x k_x f^4_y -$

-$\frac{1}{32}(-3X_1 - 30X_2 - 15X_3 - 12X_4 + 12X_5 + 12X_6 + 24X_7)f^{(4)}_z k_z f^4_y$

b^Q_{SP}=

$\frac{1}{128}(3X_1 - 18X_2 + 29X_3 - 78X_4 - 12X_5 - 12X_6 + 72X_7)f^{(4)}_x k_x f^4_y -$

-$\frac{1}{32}(4X_1 + 24X_2 - 12X_3 - 16X_5 - 16X_6)f^{(4)}_z k_z f^4_y$

c^Q_{SP}=

$\frac{1}{128}(-10X_1 - 84X_2 + 34X_3 + 12X_4 + 40X_5 + 40X_6 + 48X_7)f^{(4)}_x k_x f^4_y -$

-$\frac{1}{32}(-X_1 + 6X_2 - 5X_3 + 12X_4 + 4X_5 + 4X_6 - 24X_7)f^{(4)}_z k_z f^4_y$

d^Q_{SP}= $\frac{1}{128}(-3X_1 + 18X_2 + 3X_3 - 18X_4 + 12X_5 + 12X_6 - 72X_7)f^{(4)}_x k_x f^4_y$

b^Q_{PS}=

-$\frac{1}{128}(32X_1 + 192X_2 - 32X_3 - 192X_4 - 192X_5 - 128X_6 + 192X_7)f^{(4)}_y k_z f^3_x f_z -$

-$\frac{1}{128}(64X_1 - 64X_3 + 128X_5 - 256X_6 - 384X_7)f^{(4)}_y k_z f_x f^3_z -$

-$\frac{1}{128}(-15X_1 - 6X_2 + 15X_3 + 6X_4 - 4X_5 + 60X_6 + 24X_7)f^{(4)}_y k_x f^4_x -$

-$\frac{1}{128}(48X_1 - 192X_2 - 48X_3 + 192X_4 + 192X_5 - 192X_6 - 192X_7)f^{(4)}_y k_x f^2_x f^2_z -$

-$\frac{1}{128}(16X_1 + 96X_2 - 16X_3 - 96X_4 - 96X_5 - 96X_6 + 192X_7)f^{(4)}_y k_x f^4_z$

c^Q_{PS}=

-$\frac{1}{128}(16X_1 - 96X_2 - 16X_3 + 96X_4 + 32X_5 - 64X_6 + 96X_7)f^{(4)}_y k_z f^3_x f_z -$

-$\frac{1}{128}(20X_1 + 24X_2 - 20X_3 - 24X_4 + 16X_5 - 80X_6 - 96X_7)f^{(4)}_y k_x f^-_x$

-$\frac{1}{128}(24X_1 - 24X_3 - 96X_5 - 96X_6 + 228X_7)f^{(4)}_y k_x f^2_x f^2_z$

b^Q_{PS}= -$\frac{1}{128}(3X_1 + 18X_2 + 3X_3 - 18X_4 + 12X_5 + 12X_6 - 72X_7)f^{(4)}_y k_x f^4_x$

a^Q_{PP}=

$\frac{1}{128}(48X_1 + 96X_2 - 48X_3 - 96X_4 + 96X_5 - 192X_6 - 96X_7)f^{(4)}_x k_z f^3_x f_z +$

$\frac{1}{128}(64X_1 - 64X_3 + 128X_5 + 384X_7)f^{(4)}_x k_z f_x f^3_z +$

$\frac{1}{128}(50X_1 + 132X_2 + 22X_3 + 36X_4 + 88X_5 + 88X_6 + 144X_7)f_x^{(4)}k_x f_x^4 +$

$\frac{1}{128}(72X_1 + 192X_2 + 120X_3 + 96X_5 + 96X_6 - 288X_7)f_x^{(4)}k_x f_x^2 f_z^2 +$

$\frac{1}{128}(16X_1 + 96X_2 + 48X_3 + 96X_4 - 64X_5 - 64X_6)f_x^{(4)}k_x f_z^4$

$\frac{1}{32}(3X_1 + 30X_2 + 15X_3 + 12X_4 - 12X_5 - 12X_6 + 24X_7)f_z^{(4)}k_z f_x^4 +$

$\frac{1}{32}(24X_1 + 24X_3 + 48X_4 + 96X_7)f_z^{(4)}k_z f_x^2 f_z^2 +$

$\frac{1}{32}(8X_1 + 48X_2 + 8X_3 + 32X_5 + 32X_6)f_z^{(4)}k_z f_z^4 +$

$\frac{1}{32}(12X_1 + 24X_2 - 12X_3 - 24X_4 + 48X_5 + 24X_6 - 24X_7)f_z^{(4)}k_x f_x^3 f_z +$

$\frac{1}{32}(16X_1 - 16X_3 + 32X_6 + 96X_7)f_z^{(4)}k_x f_x f_z^3$

$b_{PP}^Q =$

$\frac{1}{128}(64X_1 - 64X_3 - 384X_5 + 128X_6)f_x^{(4)}k_z f_x^3 f_z +$

$\frac{1}{128}(64X_1 - 64X_3 + 128X_5 - 256X_6 - 384X_7)f_x^{(4)}k_z f_x f_z^3 +$

$\frac{1}{128}(-45X_1 + 78X_2 + 13X_3 + 18X_4 + 52X_5 + 52X_6 + 72X_7)f_x^{(4)}k_x f_x^4 +$

$\frac{1}{128}(96X_1 - 576X_2 + 96X_3)f_x^{(4)}k_x f_x^2 f_z^2 +$

$\frac{1}{128}(16X_1 + 96X_2 - 16X_3 - 96X_4 - 64X_5 - 64X_6)f_x^{(4)}k_x f_z^4$

$\frac{1}{32}(4X_1 + 24X_2 - 12X_3 + -16X_5 - 16X_6)f_z^{(4)}k_z f_x^4 +$

$\frac{1}{32}(24X_1 - 96X_2 + 24X_3 - 48X_4 - 96X_7)f_z^{(4)}k_z f_x^2 f_z^2 +$

$\frac{1}{32}(16X_1 - 16X_3 + 32X_5 - 96X_6)f_z^{(4)}k_x f_x^3 f_z +$

$\frac{1}{32}(16X_1 - 16X_3 - 64X_5 + 32X_6 - 96X_7)f_z^{(4)}k_x f_x^3 f_z$

$c_{PP}^Q =$

$\frac{1}{128}(16X_1 - 96X_2 - 16X_3 + 96X_4 + 32X_5 - 64X_6 + 96X_7)f_x^{(4)}k_z f_x^3 f_z +$

$\frac{1}{128}(30X_1 - 36X_2 - 6X_3 - 36X_4 - 24X_5 - 24X_6 - 144X_7)f_x^{(4)}k_x f_x^4 +$

$\frac{1}{128}(24X_1 - 24X_3 - 96X_5 - 96X_6 + 288X_7)f_x^{(4)}k_x f_x^2 f_z^2 +$

$\frac{1}{32}(X_1 - 6X_2 + 5X_3 - 12X_4 - 4X_5 - 4X_6 + 24X_7)f_z^{(4)}k_z f_x^4 +$

$\frac{1}{32}(4X_1 - 24X_2 - 4X_3 + 24X_4 - 16X_5 + 8X_6 + 24X_7)f_z^{(4)}k_x f_x^3 f_z$

$d_{PP}^Q = \frac{1}{128}(-3X_1 + 18X_2 + 3X_3 - 18X_4 + 12X_5 + 12X_6 - 72X_7)f_x^{(4)}k_x f_x^4$

The coefficients for Si(111) quadrupole contribution are given by:

$b^Q_{SS}= \frac{\sqrt{2}}{36}(5X_1+6X_2-5X_3-6X_4-20X_5+4X_6-24X_7)f_y^{(4)}k_zf_y^4$

$c^Q_{SS}= \frac{1}{36}(-X_1+6X_2+X_3-6X_4+4X_5+4X_6-24X_7)f_y^{(4)}k_xf_y^4$

$a^Q_{SP}=$

$\frac{1}{36}(2X_1+24X_2+16X_3+30X_4-8X_5-8X_6-24X_7)f_x^{(4)}k_xf_y^4+$

$\frac{1}{12}(2X_1+12X_2+4X_3+6X_4-8X_5-8X_6)f_z^{(4)}k_zf_y^4$

$b^Q_{SP}= \frac{\sqrt{2}}{12}(-X_1-6X_2+X_3+6X_4+4X_5+4X_6)(f_x^{(4)}k_z+f_z^{(4)}k_x)f_y^4$

$c^Q_{SP}= \frac{1}{36}(X_1-6X_2-X_3+6X_4-4X_5-4X_6+24X_7)f_x^{(4)}k_xf_y^4$

$b^Q_{PS}=$

$\frac{-1}{6\sqrt{2}}f_y^{(4)}(X_1+6X_2-X_3-6X_4-4X_5-4X_6)k_zf_x^4+$

$\frac{-2}{3\sqrt{2}}f_y^{(4)}(X_1-X_3+2X_5-4X_6-6X_7)k_xf_x^3f_z+$

$\frac{-2}{3\sqrt{2}}f_y^{(4)}(X_1-3X_2-X_3+3X_4+2X_5-4X_6)k_zf_x^2f_z^2+$

$\frac{-4}{9\sqrt{2}}f_y^{(4)}(X_1+3X_2-X_3-3X_4-4X_5-4X_6+6X_7)k_xf_xf_z^3$

$c^Q_{PS}= -\frac{1}{36}(X_1-6X_2-X_3+6X_4-4X_5-4X_6+24X_7)f_y^{(4)}k_xf_y^4$

$a^Q_{PS}=$

$\frac{1}{36}(24X_1-24X_3-24X_5+48X_6+72X_7)f_x^{(4)}k_zf_x^3f_z+$

$\frac{1}{36}(16X_1+48X_2-16X_3-48X_4+80X_5-16X_6-48X_7)f_x^{(4)}k_zf_xf_z^3+$

$\frac{1}{36}(10X_1+48X_2+8X_3+6X_4+32X_5+32X_6+24X_7)f_x^{(4)}k_xf_x^4+$

$\frac{1}{36}(36X_1-36X_2+36X_3+36X_4+72X_7)f_x^{(4)}k_xf_x^2f_z^2+$

$\frac{1}{36}(4X_1+48X_2+8X_3+24X_4-16X_5-16X_6-48X_7)f_x^{(4)}k_xf_z^4+$

$\frac{1}{36}(6X_1+36X_2+12X_3+18X_4-24X_5-24X_6)f_z^{(4)}k_zf_x^4+$

$\frac{1}{36}(24X_1+48X_3+48X_5+48X_6-144X_7)f_z^{(4)}k_zf_x^2f_z^2+$

$\frac{1}{36}(4X_1+48X_2+8X_3+24X_4+32X_5+32X_6+96X_7)f_z^{(4)}k_zf_z^4+$

$\frac{1}{36}(24X_1-24X_3+48X_5-24X_6+72X_7)f_z^{(4)}k_xf_x^3f_z+$

$\frac{1}{36}(16X_1+48X_2-16X_3-48X_4-16X_5+80X_6-48X_7)f_z^{(4)}k_xf_xf_z^3$

$b_{PS}^Q=$

$\frac{\sqrt{2}}{36}(5X_1+6X_2-5X_3-6X_4-20X_5+4X_6-24X_7)f_x^{(4)}k_zf_x^4+$

$\frac{\sqrt{2}}{36}(12X_1-36X_2-12X_3+36X_4+24X_5-48X_6)f_x^{(4)}k_zf_x^2f_z^2+$

$\frac{\sqrt{2}}{36}(20X_1-48X_2+4X_3-24X_4-8X_5-8X_6-96X_7)f_x^{(4)}k_xf_x^3f_z+$

$\frac{\sqrt{2}}{36}(8X_1+24X_2-8X_3+24X_4-32X_5-32X_6+48X_7)f_x^{(4)}k_xf_xf_z^3+$

$\frac{\sqrt{2}}{36}(8X_1-48X_2+62X_3-24X_4-8X_5-8X_6+48X_7)f_z^{(4)}k_zf_x^3f_z+$

$\frac{\sqrt{2}}{36}(5X_1+6X_2-5X_3-6X_4+4X_5-20X_6-24X_7)f_z^{(4)}k_xf_x^4+$

$\frac{\sqrt{2}}{36}(12X_1-36X_2-12X_3+36X_4-48X_5+24X_6)f_z^{(4)}k_xf_x^2f_z^2$

$c_{PS}^Q=\frac{1}{36}(X_1-6X_2-X_3+6X_4-4X_5-4X_6+24X_7)f_x^{(4)}k_xf_x^4$

Bibliography

[1] N. Bloembergen, Nonlinear Optics, Redwood City, Calif., 1992(1965)

[2] R. W. G. Wyckoff, Structure of Crystals, New York 1931

[3] Y. R. Shen, The Principles of Nonlinear Optics, New York 1984

[4] S. Kelykh, Nelineinaya Molekulyarnaya Optica (Nonlinear Molekular Optics), Nauka, Moscow (1981)

[5] O.A. Aktsipetrov, I.M. Baranova, and Yu.A. Il'inskii, Sov. Phys. JETP 64 (1), 167 (1986)

[6] I. Kamiya, D.E. Aspnes, L.T. Florez, J.P. Harbison, Phys. Rev. B 46, 15894 (1992)

[7] N. Bloembergen and P.S. Pershan, Phys. Rev. 128 (2), 606 (1962)

VITA

Roland Kempf was born in Alzenau, Germany, on May 28, 1974, the son of Rosa and Burkhard Kempf. After receiving his *Allgemeine Hochschulreife* at the Spessartgymnasium Alzenau in 1993 and doing his civil service at the *Ökumenische Wohnungslosenhilfe Hanau*, he entered the University of Würzburg, where he received his *Vordiplom* in physics and mathematics in 1996. In August 1997 he entered the Graduate School at The University of Texas.

Permanent Address: Kettelerstrasse 32
63776 Mömbris
Germany

This thesis was typed by the author.